Bird detection algorithm

Precious Jatau

University of Oklahoma, Cooperative Institute for Mesoscale Meteorological Studies, Norman, Ok.
University of Oklahoma, Advanced Radar Research Center, Norman, Ok.

Valery Melnikov

University of Oklahoma, Cooperative Institute for Mesoscale Meteorological Studies, and NSSL.

Table of Contents

1. Introduction

Bird strikes are a hazard for aviation. They are defined by the Federal Aviation Administration (FAA) as collisions between a bird and an aircraft resulting in the injury/death of the bird, damage of the aircraft or both (Seidenman and Spanovich 2016). According to the National Wildlife Strike Database (Federal Aviation Administration, 2016), the number of reported annual strikes has increased 7.4 times from 1,847 in 1990 to a record 13,795 in 2015. Within this timeframe, 169,856 strikes were reported either as happened in the USA or by U.S. registered aircraft in foreign countries. Birds accounted for 95.8 percent of the 2015 reported strikes. Perhaps the most high-profile incident occurred on 15 January 2009. The US Airways Flight 1549 encountered a flock of Canada Geese shortly after takeoff from the New York City LaGuardia Airport. Some birds were ingested into both engines leading to loss of thrust. Luckily, the pilots successfully landed the airplane on the Hudson River saving the lives of all 155 people on board.

Results of radar bird detection algorithm can be used for two major applications. The first is for aviation to detect areas of birds to help with avoiding bird strikes with aircrafts. The second application is for detecting situations with low bird contamination. In such a case, radar echoes are from insects and clear air returns (Bragg scatter) and the Doppler velocity field can be used to correctly obtain the wind not contaminated with strong bird velocities. Correct radar identifications of birds and insects in the atmosphere is also useful for many non-meteorological applications such as ecology, ornithology, and entomology. Such applications could increase the use of the WSR-88D data.

The WSR-88D delivers six variables: reflectivity (Z), Doppler velocity (V), spectrum width (W), differential reflectivity (Z_{DR}), differential phase (Φ_{DP}), correlation coefficient (ρ_{hv}), and specific differential phase (K_{DP}). All these variables can be used in a bird detection algorithm. The criteria of using these variables in an algorithm is discussed in the next section. Jatau and Melnikov (2019) have designed an algorithm for distinguishing bird and insect radar echoes, which uses some of the radar variables and the texture of the variables. It was noted in that algorithm that polarization properties of atmospheric biota depends on range from radar that could mean that various species fly at different heights because the radar range is directly connected to heights in radar observations. Thus, the range from radar can be an additional input variable to a bird detection algorithm.

The polarization properties of atmospheric biota depend on radar azimuth. This dependence is caused by the shapes of birds and insects and their orientation relative to the radar beam. Orientations of species depend on the wind. To account for changing wind directions, the polarization properties of biota echoes should be considered relative to the main orientations of the scatterers. That is, orientation of the species can be considered as an input parameter to the algorithm. This feature is discussed in the next section. In this project, we devised a method for converting radar measurements from being relative to the radar to be relative to the target by leveraging cases of migration toward a known direction.

In the algorithm by Jatau and Melnikov (2019), the membership function approach was used. Two algorithms presented in this report are based on machine learning approaches. The first algorithm uses the

ridge regression approach and the second one is based on decision trees. The input variables for these algorithms and their implementation are discussed in the next section. The machine learning algorithms require training and test data sets, which are presented below with a detailed description of the machine learning methods. The obtained results from the two algorithms are compared and conclusions are presented in section 6.

2. Processing features for biological targets

2.1. The input algorithm variables

The WSR-88D is capable of detecting a single biota echo up to a range of 200 km from the radar. However, distinguishing their taxa (birds or insects) is a challenge because they frequently have similar radar signatures. While reflectivity provides information about size of a scatterer, it is also directly proportional to their number concentration in the radar resolution volume. A high reflectivity value could indicate a larger target (like a bird) or a dense aggregation of small targets (insects). Because of this ambiguity, reflectivity was excluded from the input to this version of the algorithm.

Birds are larger and can fly faster than insects. While both animals will leverage the wind velocity to aid their flight, birds would be expected to have less reliance on the wind. It would make sense to use these features for separating bird and insect echoes. Radial velocity is a projection of target velocity on the radar beam. Since biological targets often take advantage of the wind velocity, it is difficult to know how much of the measured radial velocity is generated by the targets themselves. Insects can be measured at higher velocities on windy days while birds can be measured at lower velocities when the wind field is mild. The Doppler velocity was also excluded as an input to the algorithm due to this limitation for different target flight directions and underlying wind fields though still used for VAD analysis to reorient variables relative to the target's aspect. Spectrum width is also not used because of high noise contamination.

Another factor that motivated the exclusion of the legacy radar products is volume coverage pattern of NEXRAD. Birds and insects are most common at the lowest elevation ($\sim 0.5°$) scan. At this elevation, the radar completes 2 sweeps, each about 30 seconds apart. The first sweep (surveillance mode) measures the dual polarization variables and Z, while the next sweep (Doppler) collects the legacy radar products. Assuming a target flies with a radial velocity of 10 m/s, it would have migrated about 300m between both sweeps, more than the length of one range gate. The measurements from only the surveillance scan ~~is~~ are used to ensure temporal coherence.

Birds and insects frequently orient themselves relative to the wind, especially during migration. The wind changes its directions in time and height. To account for changing winds, polarimetric variables should be considered relative to orientations of birds and insects. To do so, the direction of migration has been obtained for every range interval using VAD analysis. A left shift is then performed to normalize the radar variables relative to the target aspect. Aspect averaging is then applied to improve the signal to noise ratio (SNR). To account for the azimuthal dependence of the dual-pol radar variables, 18 azimuthal sectors have been created in the whole 360^o field (Fig. 1) so that the width of an azimuthal sector is 20^o. Each azimuthal sector represents a target aspect. The radar distance has been also divided into 10 km long range intervals (Fig. 1). Radar data from the first range interval have not been used because of strong contamination from ground clutter (the empty smallest circle in Fig. 1). The final variables used in training the classifiers are the dual polarization variables, their textures, range, and target aspect. Dual pol variables are used because

they are robust to differing target size and concentration. They also provide information on the shape and uniformity of the targets.

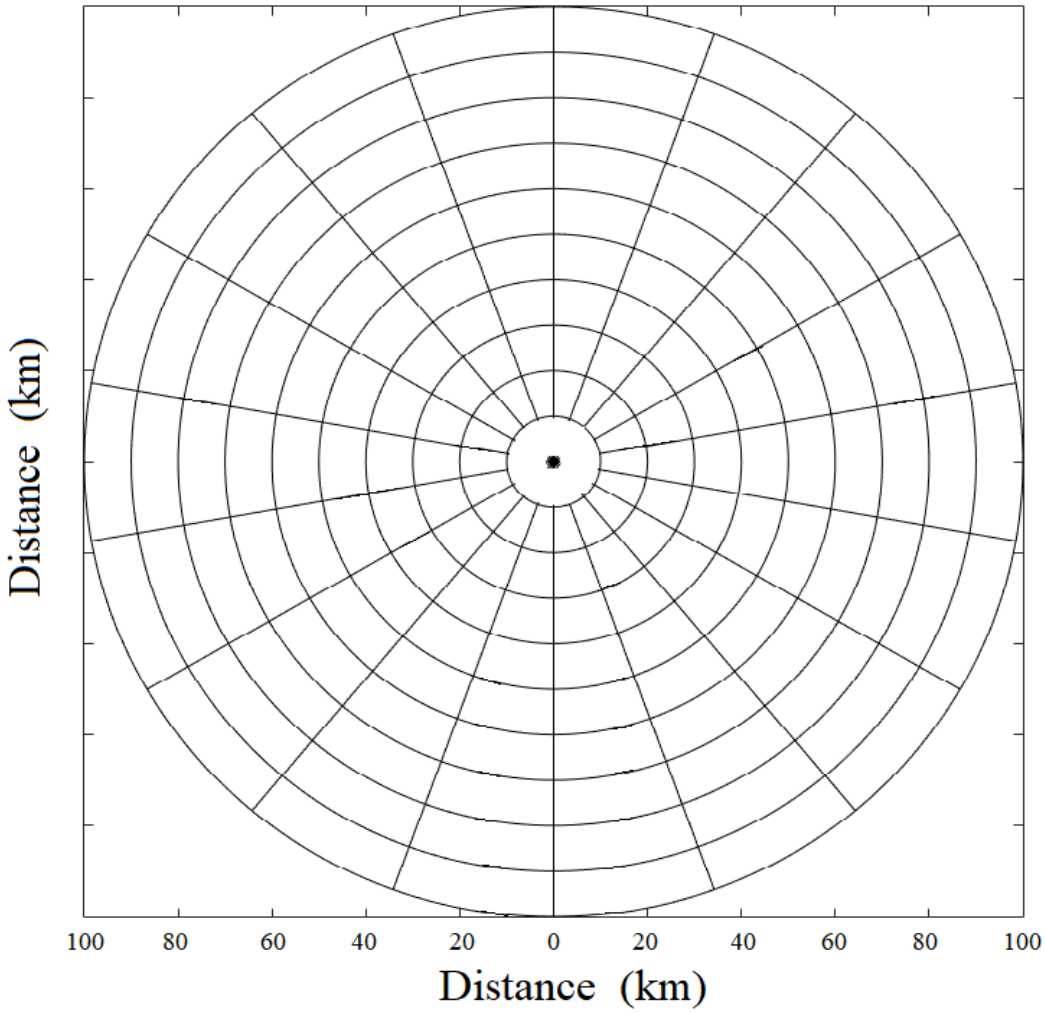

Fig. 1. Layout of the range intervals and azimuthal sectors used in the algorithms.

2.2. Blob coloring with minor region removal

Blob coloring is a low-level image processing step performed prior to some higher-level computer vision process. It is usually performed to extract an object against a back ground. Objects (or regions) are defined as connected target pixels in the image surrounded by background. They are identified by iterating over the image in raster scan order with a 3 by 3 filter that assigns a unique number to each region. Surroundings were defined using a 4 connected neighborhood (Bovic, 2009). After the first pass of the algorithm, several blobs would be identified. Each blob has a count for the number of pixels (or range gates) that it covers. The blob with the largest count is kept and all other blobs deleted. Usually the coloring process is imperfect leaving with some holes in the target blob. This is addressed by inverting the image, repeating the coloring process, extracting the largest blob again and finally re-inverting the image (Bovic, 2009).

Radar data from insects and birds were collected for clear air days with minimal precipitation contamination, thus the biggest object in this case is always the migration echoes centered at the radar

location. Figure 2 shows an example of a bird migration contained within a range of about 150 km. Let this original image be I. A new binarized image is obtained setting the background pixels to zero and non-background pixels to 1. The result is a large connected region close to the radar location and more isolated regions at the fringe of the echo. The binarized image is dilated twice to join the isolated region to the main echo. The new dilated image J is given as

$$J = (I \oplus B) \oplus B \qquad (1)$$

Where B is the 3 by 3 window, and $\oplus$ represents the dilation operation.

Next, blob coloring with minor region removal is performed on J to get a map M of the target, shown in figure 3. The final extracted image K of the radar echo (fig 4) is obtained by element wise multiplication of the original image and the target map

$$K = I \odot M \qquad (2)$$

The same procedure was repeated to extract the insect echo. Fig. 5 shows the original image of insect reflectivity. This case had a little contamination from weather seen west of the insect migration echoes. Blob coloring with minor region removal excludes this contamination. The map of the region of interest can be seen in figure 6. The final extracted image (fig 7) is less noisy recovering only the insect echoes.

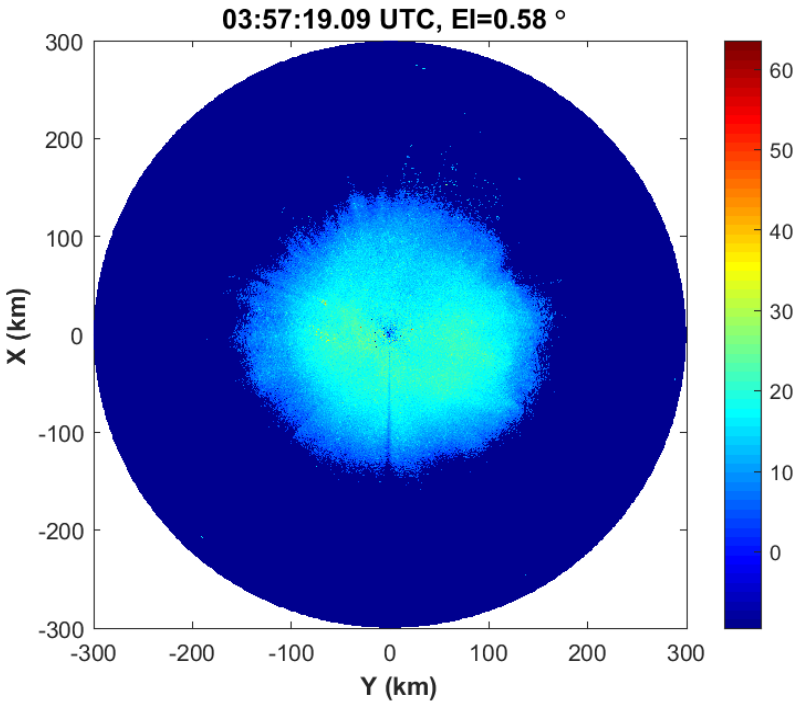

Figure 2: Reflectivity Z of bird migration echo

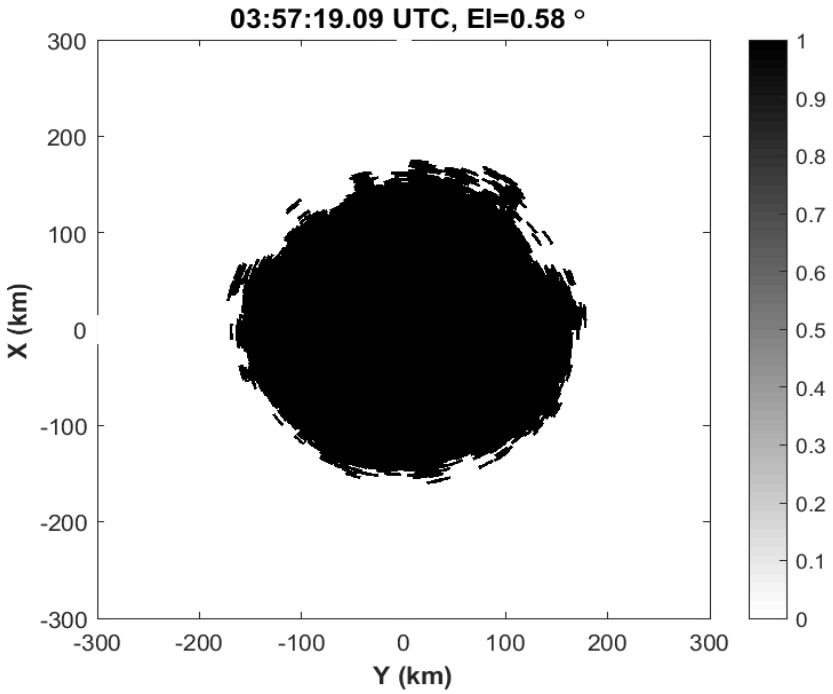

Figure 3: Mask of major region extracted by blob coloring algorithm

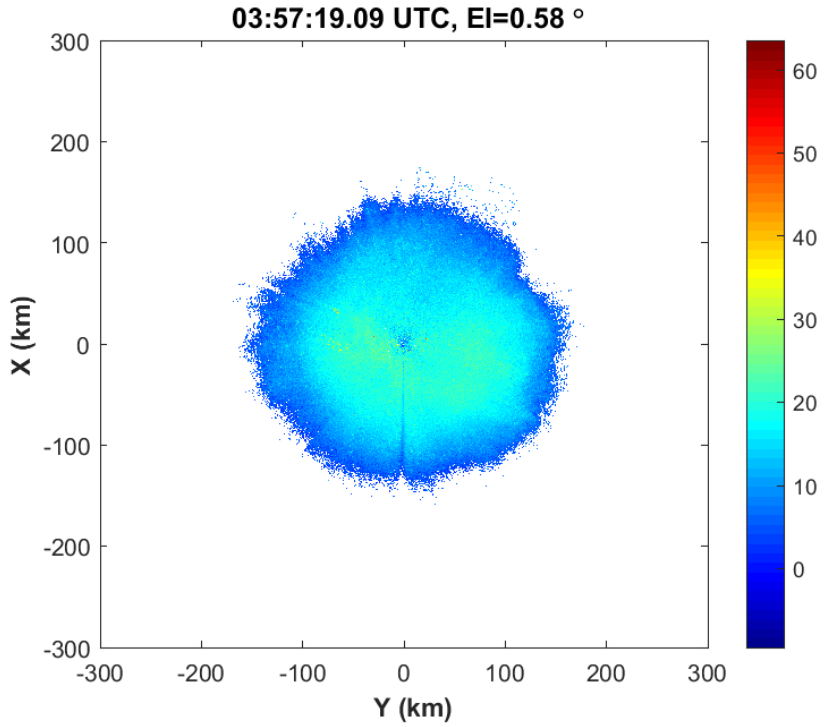

Figure 4: Reflectivity of extracted bird migration echo

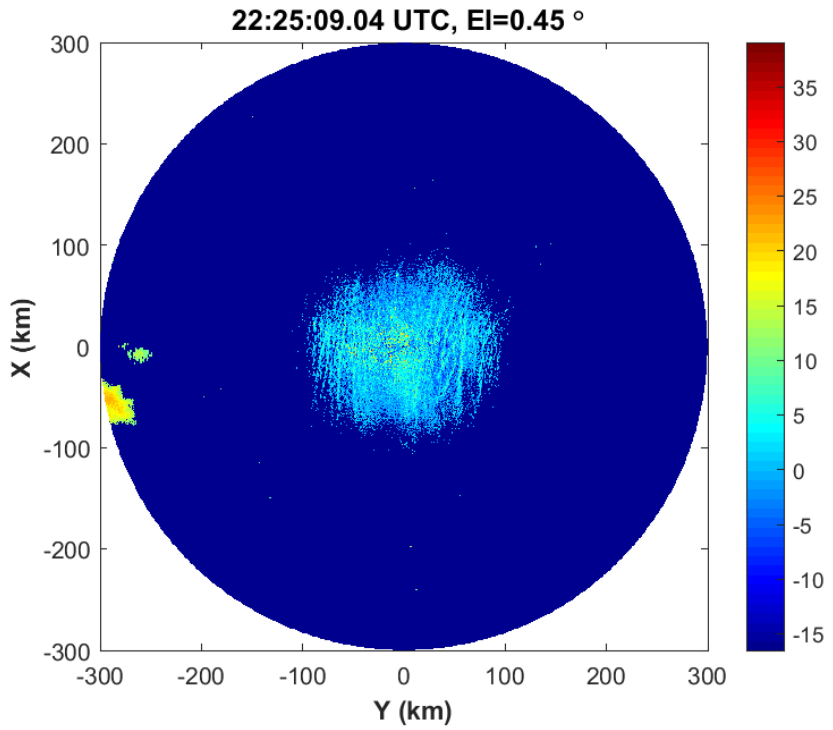

Figure 5: Reflectivity of insect migration echo

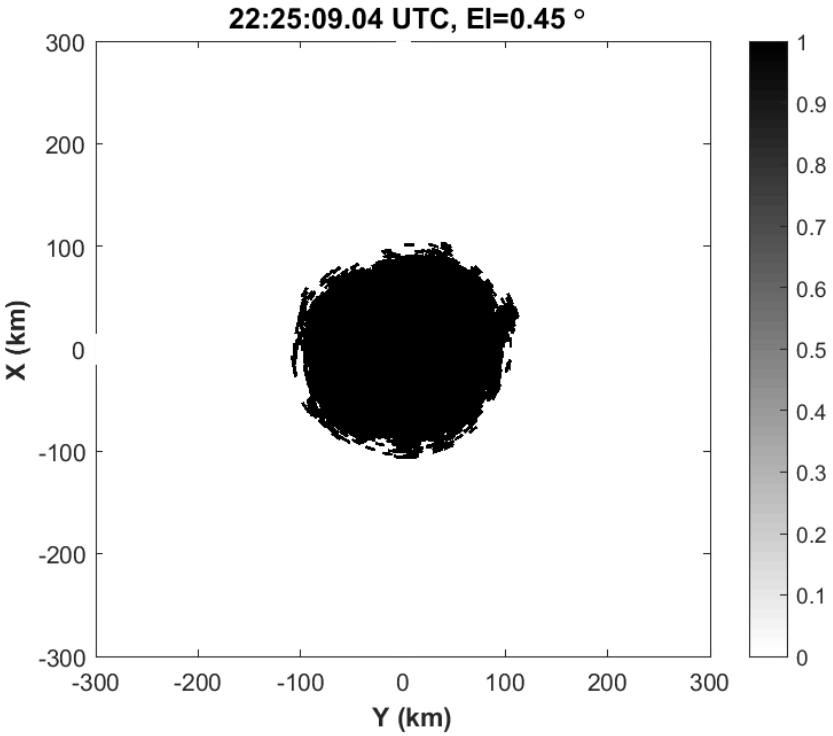

Figure 6: Mask of major region extracted by blob coloring

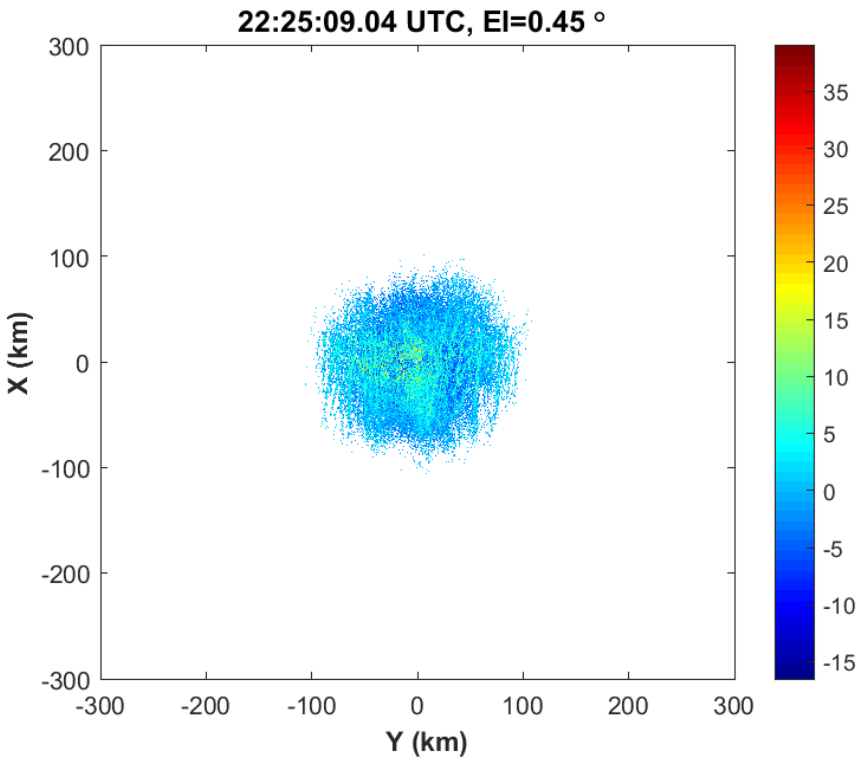

Figure 7: Reflectivity of extracted insect migration echo

2.3. Texture

Texture gives information about the variation of radar products over a 3 by 3 range gate window. The window is slid across the image in raster scan order, and the mean absolute difference of the 8 surrounding gates from the reference gate is output (Jatau and Melnikov, 2019). Edge effects along the azimuth are handled by periodic extension. There are no edge effects for range because our analysis starts from 10 km and never uses the full range extent. Calculations were also confined to only gates that have targets present in all 8 neighbors in a star neighborhood topology. Mathematically, texture is given as

$$\Delta x_{ab} = \frac{1}{N-1}\sum_{i=-1}^{+1}\sum_{j=-1}^{+1}|x_{ab} - x_{a+i,b+j}| \quad (3)$$

Where Δx_{ab} is the texture of product x at range gate a and azimuth b.

i is the range index offset,

j is the azimuth index offset, and

N is the window size.

2.4. Reference with respect to bird/insect azimuth

Migration have been observed to have a strong azimuthal dependence due to the different aspects being sampled (Stepanian et al, 2016). This is characterized by symmetry patterns in the dual pol variables. We

explored a method for handling this dependence by reorienting radar variables relative to the target's azimuth. First, a sinusoidal model is fit to every range of the form

$$V_r(\theta_{az}) = |V|cos(2\pi f\theta_{az}) + \varphi_{phase} \quad (4)$$

Where V_r is the radial velocity, $|V|$ is the magnitude of velocity along the migration direction, f is frequency, θ_{az} is the radar azimuth (in degrees) and φ_{phase} is a phase offset. It is assumed that the wind field is uniform at every height, therefore $f \approx \frac{1}{360}$ cycles/ degree. The migration direction $\theta_{migration}$ is recovered as the angle that maximizes radial velocity,

$$\theta_{migration} = argmax_{\theta_{az}} V_r(\theta_{az}) \quad (5)$$

An example of a VAD cut for 70 km taken from KTLX on 03rd May, 2015 at 05:08:15 UTC is shown in fig 8. The blue line represents the filtered Doppler velocity while the green line represents the sinusoid fit. Migration in this case is toward $13.73°$ azimuth relative to the radar. Other markers at $103.73°$ and $283.73°$ are the zero iso-dops of velocity while $193.73°$ is the direction from which the migration originates. These azimuths also give information on the back scatter from different aspects. For example, $13.73°$ is sampling the tail aspect of the birds, $103.73°$, the left wing, $193.73°$ the head and $283.73°$ the right wing. Migration direction changes with wind, range (height) from the radar, time of day and weather. This coupled with the complex shapes of biological targets make signal processing along aspects challenging.

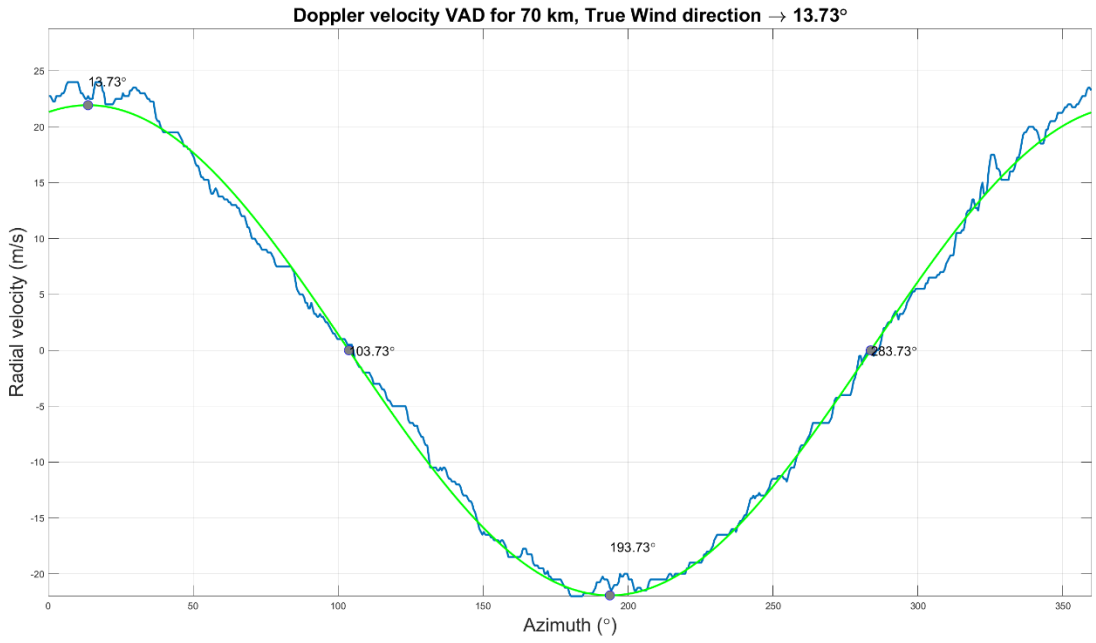

Figure 8: VAD for 70 km relative to radar

The velocity relative to the aspect of the birds (or insects) is obtained by left shifting V_r by $\theta_{migration}$

$$V_r(\theta_{aspect}) = V_r(\theta_{az} - \theta_{migration}) \quad (6)$$

The result is a radial velocity field such that $0°$ represents tail on sampling, $90°$ left wing, $180°$ head on and $270°$ right wing shown in fig. 9 below. The same shift is applied to normalize ZDR, Φ_{DP} and ρ_{HV}. Further analysis of the VAD pattern also showed that dual pol variables had little fluctuations over $20°$ sectors. Thus, range gates were aggregated into $20°$ azimuth by 10 km range-sector bins to have more measurements per bin.

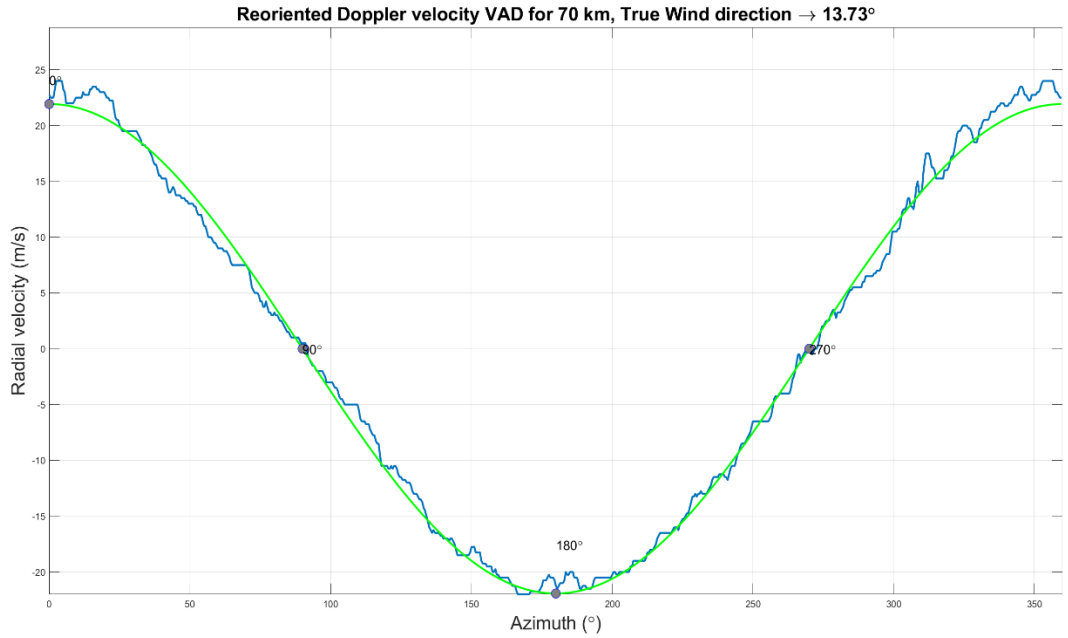

Figure 9: VAD at 70 km relative to bird aspect

3. Data analysis

3.1. Train and test data

45 cases (PPIs) of biota migration were collected from KLTX for both birds and insects. Migration echoes were extracted using blob coloring with minor region removal and labelled by their comprising scatterers. All gates that are part of a bird migration blob are labelled birds and vice versa. In reality, biota echoes are frequently cross contaminated. There will be many gates that contain both scatterers at the same time.

There will also be gates that contain insects within a bird migration blob or birds within an insect migration blob. Furthermore, verifying each individual gate will be impossible given that the data used was collected within a radius of over 200 km.

To mitigate this, further processing was applied to the data set. First, the migration direction at all ranges were recovered using VAD fit and then reoriented relative to the target azimuth. Each PPI was then randomly divided into 3 batches each containing 30 cases (15 for each class). Two batches were selected as the training set while the last batch was the test set.

The next step attempts to improve the signal to clutter ratio within each batch. For each class, all 15 cases are averaged for each range gate within $0.5°$aspect bins. For example, within a batch, all ZDR values within an aspect angle of $0^{\circ} - 0.5^{\circ}$ will be averaged to get one ZDR value. A similar process is repeated for $0.5^{\circ} - 1.0^{\circ}$, $1.0^{\circ} - 1.5^{\circ}$ and so on. The result of this step is that all 15 ppi's within one batch are averaged into 1 ppi with less contamination. The final training data contained 2 of such averaged ppi's. The test cases are kept in its original form since classification at test time will always be done for one PPI.

3.2. Results

The aspect averaging gives an insight into how the transmitted wave interacts with the complex shape of birds/insects. Fig 10 shows the averaged ZDR of the training data as a function of θ_{aspect} at ranges 15, 30, 45 and 90 km. It can be seen that ZDR generally has a sinusoidally pattern with the highest value of around 230^{o} (between the head and the right wing), and the lowest values are around 75°. The sinusoidal aspect dependence is also evident (Fig. 10 right) in the bimodal nature of the bird distributions. Insects on the other hand generally have higher values, accumulating around the $8\ dB$ limit. Other data collected from research radars have shown that insects can have ZDR up to $\boldsymbol{24\ dB}$. The clamping of values at the 8 dB limit could explain why there is not as obvious a pattern as in the bird case. Insects also have larger fluctuations which could imply that they are more sensitive to changes in viewing angle. The right part of fig. 10 also shows their distributions. Birds have most of their ZDR in the interval $(-2,4)\ dB$ while insects have values over the whole ZDR range.

More analysis was carried out to observe the distribution of radar variables over different sector range intervals shown in fig 11. From left to right the range intervals considered are 1, 3, 5 and 7. From top to bottom, the sectors considered are 1,5, 9, 14 and 18. Recall that sectors represent 20° bins of the aspect angle, so sector 1 will be for θ_{az} between $0 - 19.99^{o}$ (contains the direction of migration), sector 9 is directly opposite sector 1 and sector 18 is adjacent to sector 1. The separation between bird and insect distributions is better for sectors 5, 9 and 18. Generally, there is clearer separation when sector is incorporated in fig. 11 compared to the distributions in figure 10.

Φ_{DP} for bird echoes (fig 12) also show a pattern with peak values at about 50° and 300° . This result is consistent with the observed bilateral symmetry seen in bird migration studies (Stepanian *et al*, 2016) where there are two regions about 180° apart with high Φ_{DP} values. The minimum value across all considered ranges is found at 180° which is the head aspect of the bird. Additionally, Φ_{DP} for insects is more random possibly due to aliasing of low values into higher values. True values should be around 70°. Generally, birds can be seen (right of fig. 12) to have higher Φ_{DP} than insects. Fig 13 shows once again that using sector information enhances the separation between both classes.

ρ_{HV} for bird migration have been observed to have low values corresponding to tail-on viewing angles and high values for head on angles (Stepanian and Horton 2015, Van Den Broeke 2013). This can be seen in the sinusoid-like pattern of figure 14 with high values between 60° and 250° and low values otherwise. As a result, the distributions (figure 14, right) are strongly bimodal. Incorporating sector dissolves the bimodal distributions into the more desired normal distributions within range sector bins. Sector 1, 5 and 18 have the clearest separation between birds and insects while sectors 9 and 14 have more overlap between both classes.

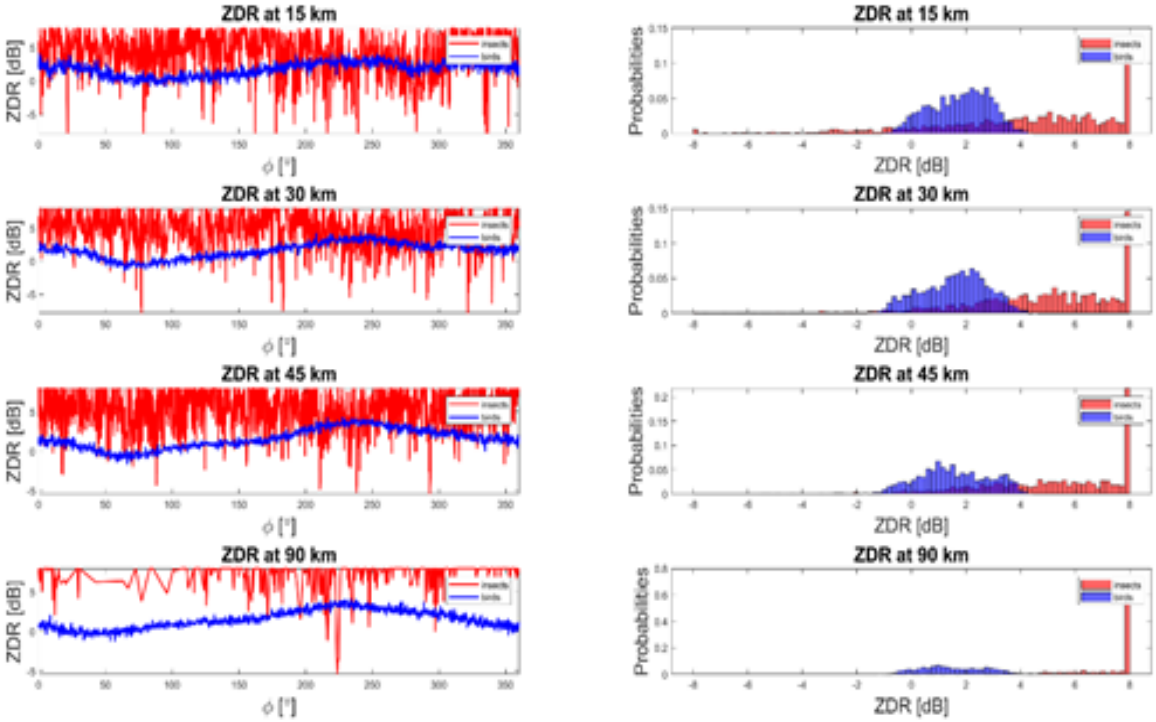

Figure 10: ZDR as a function of aspect angle (left) and distribution of ZDR (right) at 15, 30, 45 and 90 km. The insect data are in red and bird data are in blue.

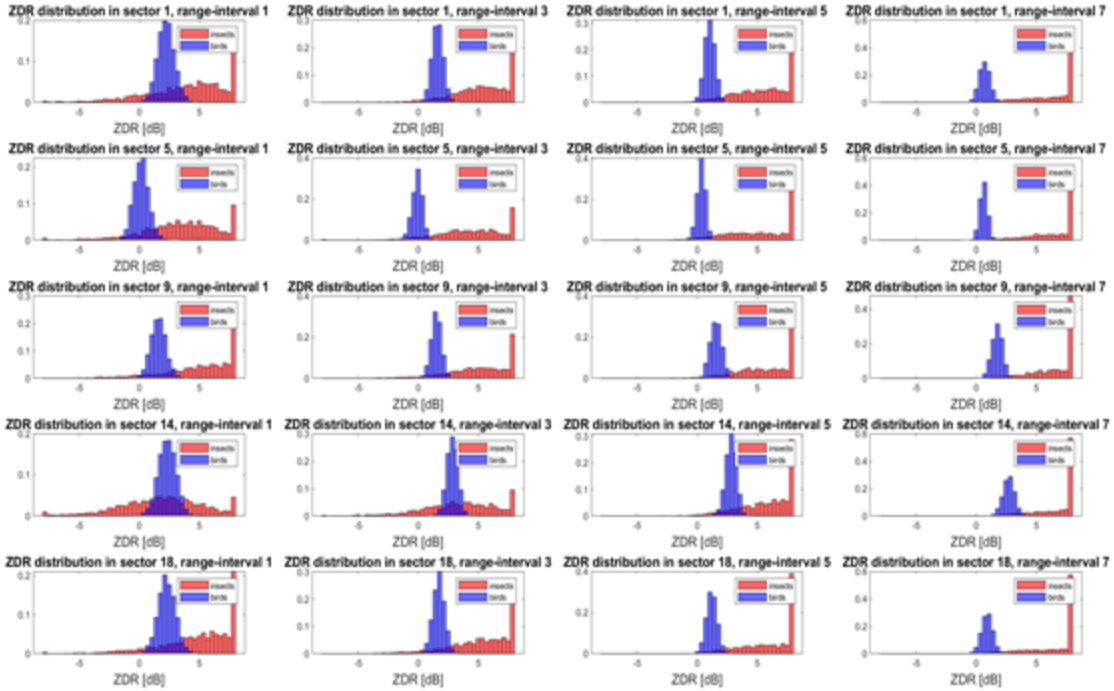

Figure 11: Distribution of ZDR at range interval 1,3,5 & 7 and sectors 1,5,9, 14 & 18. Insect data are in red and bird data are in blue.

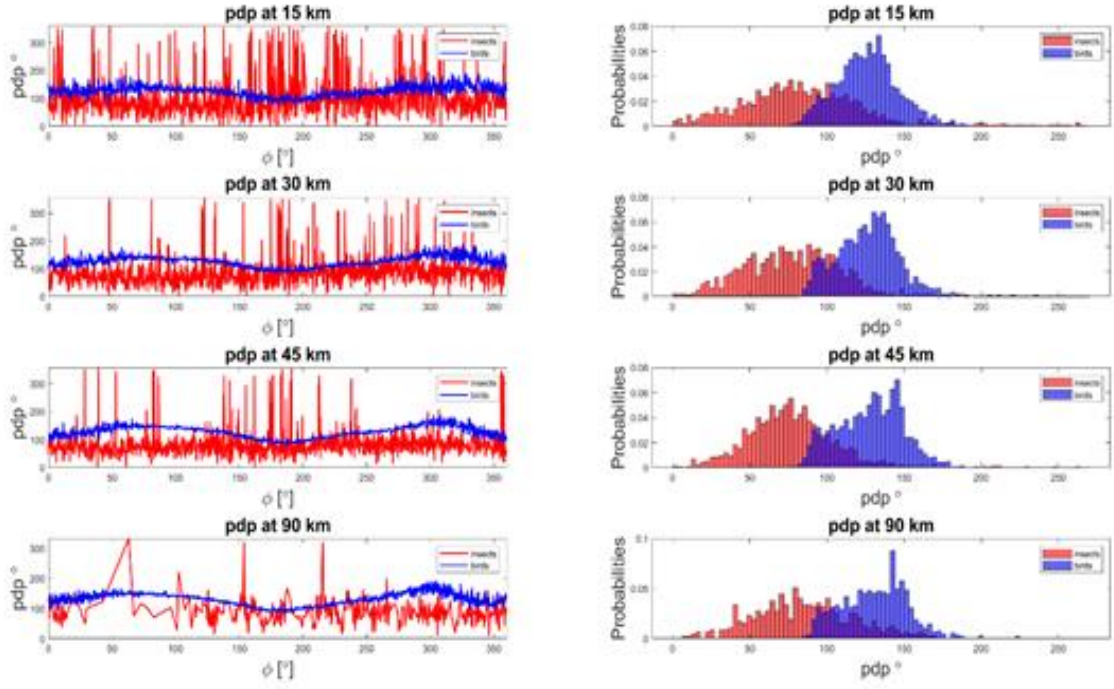

Figure 12: φ_{DP} as a function of aspect angle (left) and distribution of φ_{DP} at 15, 30, 45 and 90 km. Insect data are in red and bird data are in blue.

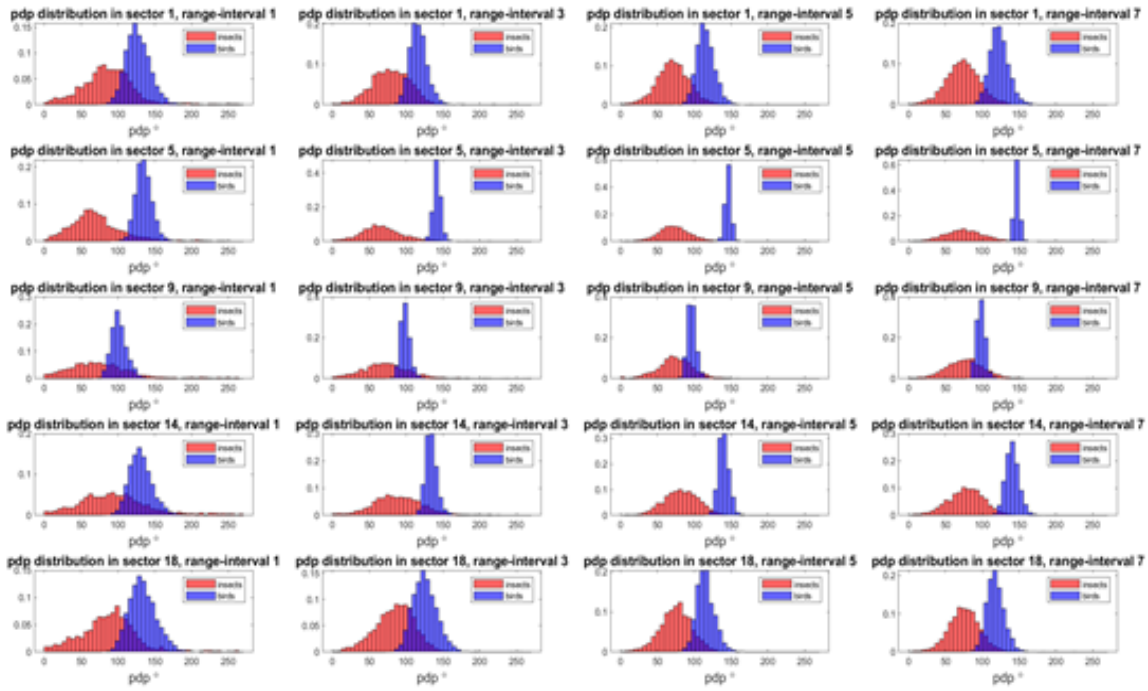

Figure 13: Distribution of φ_{DP} at range interval 1,3,5 & 7 and sectors 1,5,9, 14 & 18. Insect data are in red and bird data are in blue.

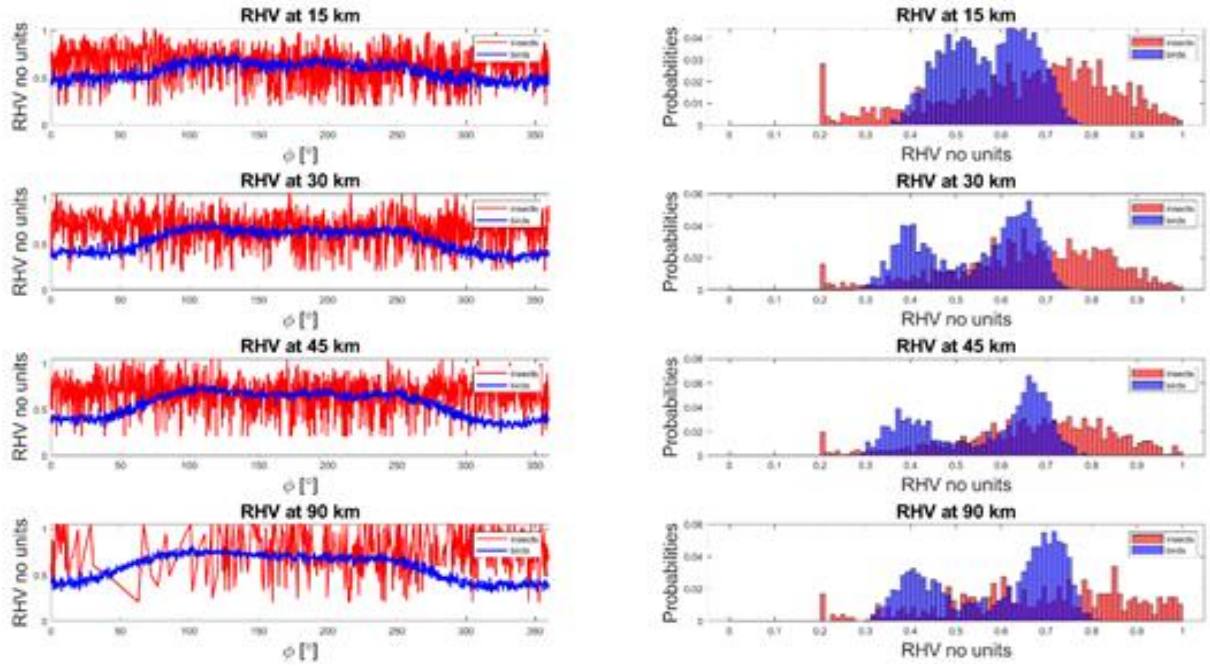

Figure 14: ρ_{HV} as a function of aspect angle (left) and distribution at 15, 30, 45 and 90 km. Insect data are in red and bird data are in blue.

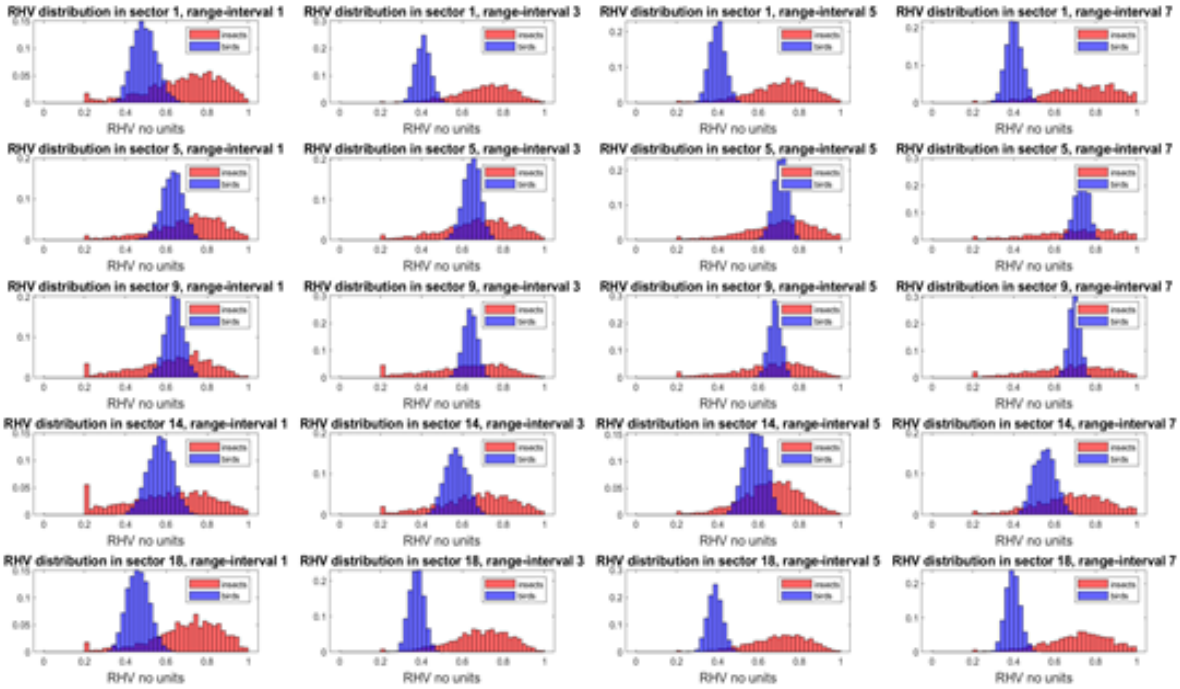

Figure 15: Distribution of ρ_{HV} at range interval 1,3,5 & 7 and sectors 1,5,9, 14 & 18. Insect data are in red and bird data are in blue.

4. Machine learning methods

4.1. Logistic regression

Logistic regression is a model for predicting a categorical variable as a function of linear combination of it's predictors. In our case, prediction is whether a range gate contains birds or insects based on the level II dual polarization variables. The predictors used are ZDR, φ_{DP}, ρ_{HV}, sector and range interval. The target variable $isBird$ is a binary label used to indicate whether the current range gate contains birds or insects. The probability of that a range gate contains bird echo μ_{isBird} is given by

$$\mu_{isBird} = \frac{1}{1 + e^{-(\beta_0 + \beta_{ZDR} ZDR + \beta_{\phi_{DP}} \phi_{DP} + \beta_{\rho_{HV}} \rho_{HV} + \beta_{sector} sector + \beta_{ri} ri)}} \qquad (7)$$

Where $\beta's$ are weights given to each variable and *ri* stands for range interval. Final classification is made for birds if μ_{isBird} exceeds a threshold of 0.5 and insects otherwise. This will be a binary outcome, though we can alternatively just consider the probabilities depending on the desired application. Logistic regression is trained by finding weights that minimize the root mean squared error e defined as

$$e(\beta_j) = \sqrt{\frac{\sum(y_i - \hat{y}_i)^2}{n}} \qquad (8)$$

Where y_i is the label provided for whether a gate contains birds (1) or insects (0), and $\hat{y}_i$ is the predicted outcome.

In this project, we used ridge regression which uses an additional regularization hyperparameter λ on normal logistic regression that penalizes overconfident weighting on predictors. The modified loss function $L(\beta_j)$ will be

$$L(\beta_j) = e(\beta_j) + \lambda \sum_{j=1}^{p} \beta_j^2 \quad (9)$$

Training in this case involves finding both β's and λ that minimizes this loss function. Ridge regression was executed using the glmnet (**Friedman et. al, 2010)** and ipflasso (**Boulesteix and Fuchs, 2019)** in R programming language.

4.2. Decision trees

Decision trees uses a combination of thresholds on the predictor variables to divide data so that subsets are as homogenous as possible. They are formed by hierarchy of parent nodes and children nodes. Another way to understand the tree is using root, decision and leaf nodes. The root node is exclusively a parent node. Decision nodes are both parents and children, while leaf nodes are exclusively children.

There are many loss functions used to guide the splitting on the trees. In this project, we wanted to maximize information gain thereby minimizing the entropy of children nodes. Entropy measures the homogeneity of a node. The entropy of a single variable $E(x)$ defined as

$$E(x) = -\sum_i p_i \, log_2 \, p_i \quad (10)$$

where p_i is the probability of the ith class.

Consider a split on variable x_1 that have classes true and false. If it produces a node with 99% true and 1% true respectively, the entropy will be $E(x_1) = -0.99 \times log_2 0.99 - 0.01 \times log_2 0.01 = 0.08$. It is almost zero because the children nodes are almost pure. Alternatively, an impure split 50-50 split would have a high entropy.

Entropy at nodes in decision trees defined relative to the target variable T given as

$$E(T, X) = \sum_{C \in X} p(c) E(c) \quad (11)$$

Where X is the current variable. Information gain G of a split measures the reduction in entropy relative to the target class. It is given as

$$G(T, X) = E(T) - E(T, X) \quad (12)$$

Growing the decision tree at every node involves analyzing the information gain of possible splits. The one with the highest gain is always executed first. Splitting continues recursively until the final leaf nodes are sufficiently pure. The rpart package (**Therneau and Atkinson, 2018)** was used for training the model.

4.3. Metrics

We used four different metrics to measure the performance of a classifier. These are accuracy ACC, true positive rate TPR, true negative rate TNR, and the area under the Receiver Operating Characteristic (ROC) curve. Table 1 below shows how this metrics are obtained for bird detection. The true label is the marker provided by Jatau and Melnikov to indicate whether a range gate contains bird or non-bird echo. After training, the classifier is applied to predict the already labelled gates. The number of gates that are labelled as birds and predicted as birds make up the true positive (TP) cases. Gates that are labelled as birds but are predicted as insects are false negatives (FN). Gates that are labelled as insects and predicted as insects are true negatives (TN). Finally, gates that are labelled as insects but predicted as birds are false positives (FP). Three metrics are calculated as

Classifier output	True label	
	Birds	Insects
Birds	True Positives (TP)	False Positives (FP)
Insects	False Negatives (FN)	True Negatives (TN)

Table 1: Confusion matrix for bird detection

$$ACC = \frac{TP+TN}{TP+FN+FP+FN} \quad (13)$$

$$TPR = \frac{TP}{TP+FN} \quad (14)$$

$$TNR = \frac{TN}{FP+TN} \quad (15)$$

In practice, values close to 1 are desirable for this metrics. These metric were calculated using the caret package (Khun *et al*, 2019). The ROC curve plots the TPR against $1 - TNR$ (or False Positive Rate FPN) for different thresholds on the probability of birds and insects. An example of the ROC curve for the ridge regression model using Φ_{DP}, ρ_{HV}, and sector is shown in figure 16. This curve was generated using the ROCR package (Sing *et al*, 2005). The left side of the figure represents a threshold on the probability of birds close to 1. This strict threshold will detect no insects and only a few gates with very high probability of birds. Moving right along fig 16 signifies decreasing the threshold toward zero. The lower probability threshold on the other hand detects almost all bird gates but also misclassifies a huge portion of insect gates. The diagonal line signifies random chance. A metric used to summarize the ROC curve is called the Area Under Curve (AUC) which is calculated as the name implies. An ideal classifier will have the elbow of the ROC curve close to the top left corner and an AUC of 1 while a random chance model will have an AUC of 0.5 (**Fawcett, 2006)** with the ROC curve tracing a diagonal.

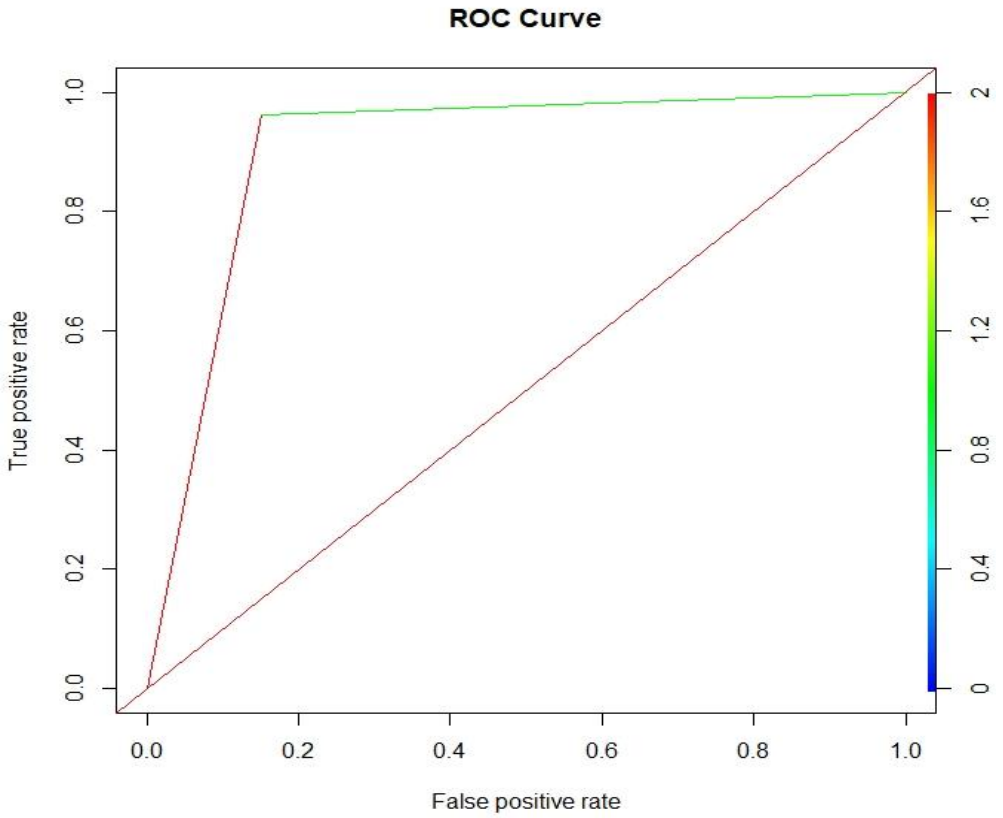

Figure 16: ROC curve for ridge regression model using φ_{DP}, ρ_{HV}, and sector.

5. Performance

The classification metrics for the ridge regression and decision tree classifiers on the test set are shown in table 2 below. They are based on the labels provided for the extracted migration echoes. Recall that all gates within a bird migration blob for example are labelled birds though in practice, such blobs will also contain insects. These insects, if detected by the classifier will be wrongly considered as a misclassification. As a result, the metrics obtained will be an approximation. We believe that the true performance of the some of these classifiers is better than the metrics will lead us to believe. The final decision on which classifiers should be used will be a result of combined analysis on these metrics and the performance on qualitative validation cases.

Different models were explored because not all predictors can be obtained in real time situations. For example, sector depends on a sinusoid fit on the velocity of migration echoes. So, in non-migration cases or even migration cases with heavy velocity aliasing, it will be difficult to obtain sector. Additionally, our calculation of texture depends on the current gate having targets present in all 8 neighboring gates. Texture cannot be obtained in an alternative scenario.

Comparison of the two algorithms show that decision tree models with range interval performs best on insect cases (having TNR ≥ 0.93). This is because the algorithm learns a range threshold (~ 100 km) such that all gates below this range are classified as insects, with birds classified otherwise. This decision node makes sense because insects are in fact found at lower ranges. However, the rigid binary threshold will

result in many birds at low altitudes being misclassified. The effect is a worse performance on bird cases, with a maximum TPR of 0.75.

	ACC	TPR	TNR	AUC
Ridge regression				
Dual pol (Z_{DR}, Φ_{DP}, ρ_{hv})	0.80	0.82	0.76	0.85
Dual pol + texture	0.86	0.87	0.84	0.92
Dual pol + sector	0.82	0.85	0.77	0.86
Dual pol + range interval	0.81	0.79	0.84	0.89
Dual pol + texture + sector	0.87	0.88	0.85	0.92
Dual pol + sector + range interval	0.82	0.80	0.84	0.89
Dual pol + texture + range interval	0.88	0.87	0.91	0.94
Dual pol + texture + sector + range interval	0.88	0.87	0.91	0.94
Decision trees				
Dual pol (Z_{DR}, Φ_{DP}, ρ_{hv})	0.73	0.68	0.86	0.87
Dual pol + texture	0.79	0.75	0.89	0.89
Dual pol + sector	0.73	0.68	0.88	0.87
Dual pol + range interval	0.69	0.60	0.93	0.88
Dual pol + texture + sector	0.79	0.75	0.89	0.89
Dual pol + sector + range interval	0.71	0.61	0.95	0.88
Dual pol + texture + range interval	0.73	0.64	0.97	0.88
Dual pol + texture + sector + range interval	0.73	0.64	0.97	0.89

Table 2: Classifier metrics on test cases

Overall ridge regression performs better than the decision trees with higher ACC, TPR and AUC. The more gradual approach of increasing bird probability every 10 km also allows for better detection of birds at low ranges while still recovering insects' echoes at a good rate. Texture has the additional effect of smoothening radar products. Models with texture generally have better metrics because test data was for migration where the windowed gates will contain similar targets. However, we believe that cases with a heterogeneous mixture of scatterers could have worse performance for models with texture.

Qualitative validation cases

In this section, the different classifiers were tested on known cases of bird and insect activity. The first two cases are for bird roosts on an insect background. Bird roosts form a good validation case because they are easily recognized in radar images. They also provide diverse scattering characteristics by providing different viewing angles to the radar. Furthermore, there were no roosts in the training set so the ability to detect them will be a good test of performance. The remaining cases are for bird and insect migration.

5.1. KHTX Bird Roost

The first case is a 0.5° elevation scan collected by KHTX on 11 August 2015 at 11:15 UTC (shown in fig 17 below) containing bird roosts. It was chosen because the scatterers have already been identified by

Stepanian *et a*l 2016. It was also obtained from a different WSR-88D so the performance of classifiers here will illustrate their capability to be used on the NEXRAD network.

Stepanian *et a*l 2016 identified three main causes of echoes for this case. First are two colonies of purple martins engaging in their morning roosts verified by ground observers from the Purple Martin Conservation Society. They are located north-west and south-west of the radar location. Second, insects were confirmed by their comparatively low mean airspeed of 1.80 m/s and concentration at lower altitudes. Air speed was calculated by vector subtraction of windspeeds obtained from balloon soundings from ground speeds obtained from radial velocity (Stepanian and Horton 2015). Finally, weather echoes were identified using their near 0 dB ZDR, near 1 ρ_{HV} and Φ_{DP} near the system calibration offset of 60°. A region of overlap between insects and weather was also identified (enclosed in the red circle, fig 17).

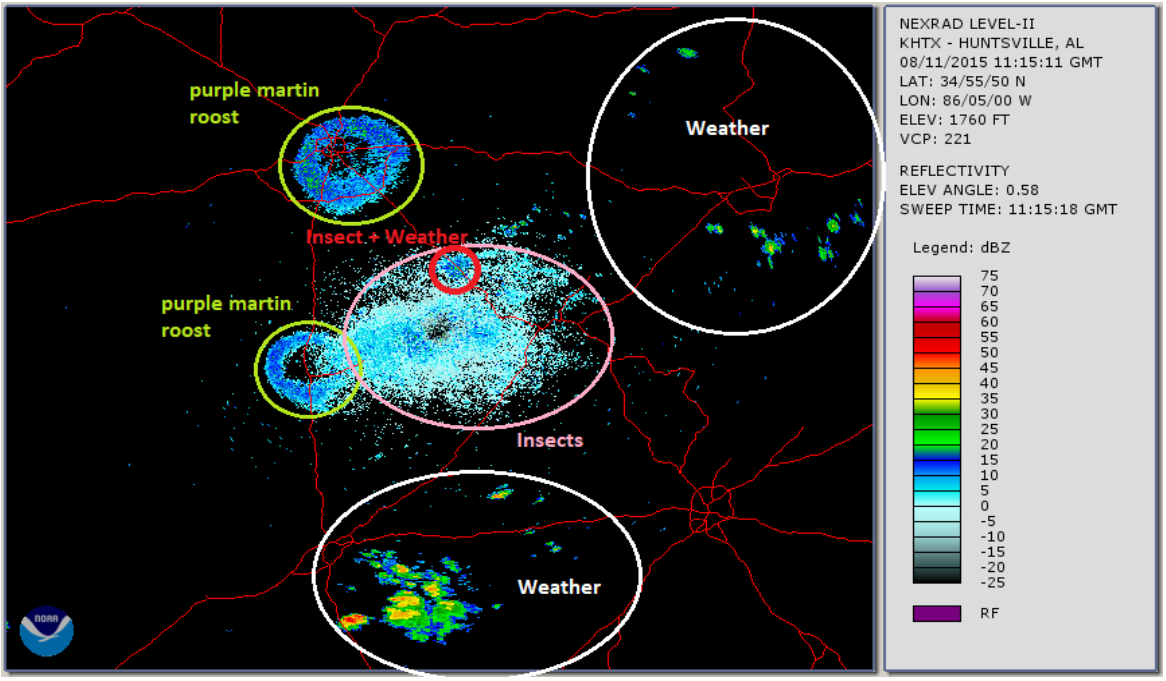

Figure 17: Reflectivity of Purple martin roosts (in light green) observed with KHTX on 11 August, 2015 at 11:15 UTC. Insects were location around the radar location (in pink). The red circle shows the region where insect and weather echoes overlap.

In this case, it is not possible to recover sector because of the presence of different targets with diverse velocities. The models without sector as inputs are therefore used. Fig 18 shows the results for using the dual pol variables and range interval. Birds are colored blue while insects are red. The ridge regression results (shown on the left) correctly identifies the rings as mostly birds and insects as mostly insects. We believe this is the best performing model. A class was not trained for weather echoes, so they tend to be misclassified as birds. This should not be a problem in practice because the model is meant to be used on the biological class identified by the hydrometeor classification algorithm. Also notice that the gates were weather and insect echoes overlap are similarly classified as birds. The decision tree results (shown on the right) picks up a larger part of the rings as insects. Classification on the insect echoes also seem more accurate. However, this is because decision trees set a range threshold around 110 km. Most echoes below

this range are classified as insects. Decision trees generally misclassify more parts of the roost (seen in fig. 18 - 21). Also, models with texture (fig 19 and 21) perform worse probably because of the heterogeneity of scatterers.

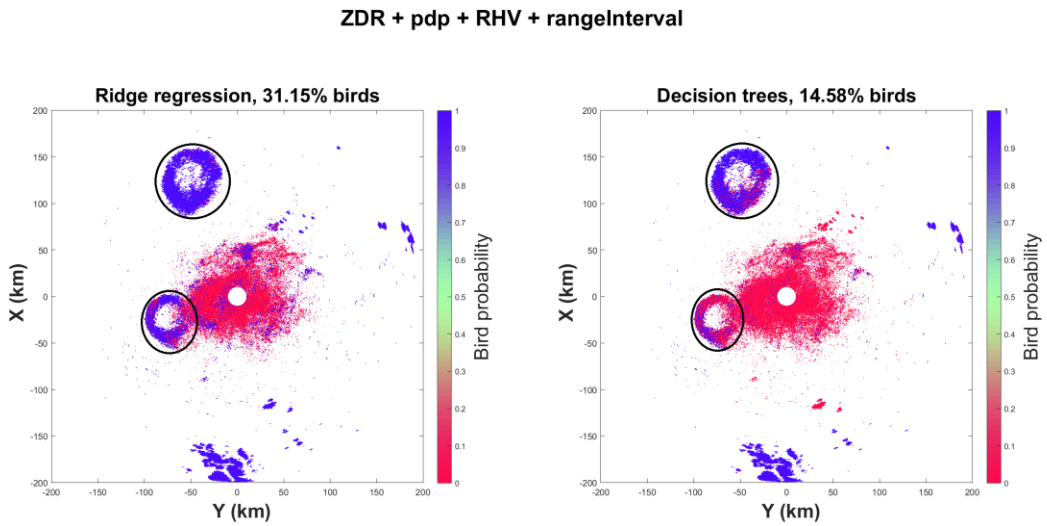

Figure 18: Ridge regression (left) and decision tree (right) classification results using dual pol variables and range interval for the case in Fig. 17. Bird roosts are enclosed in the black circles.

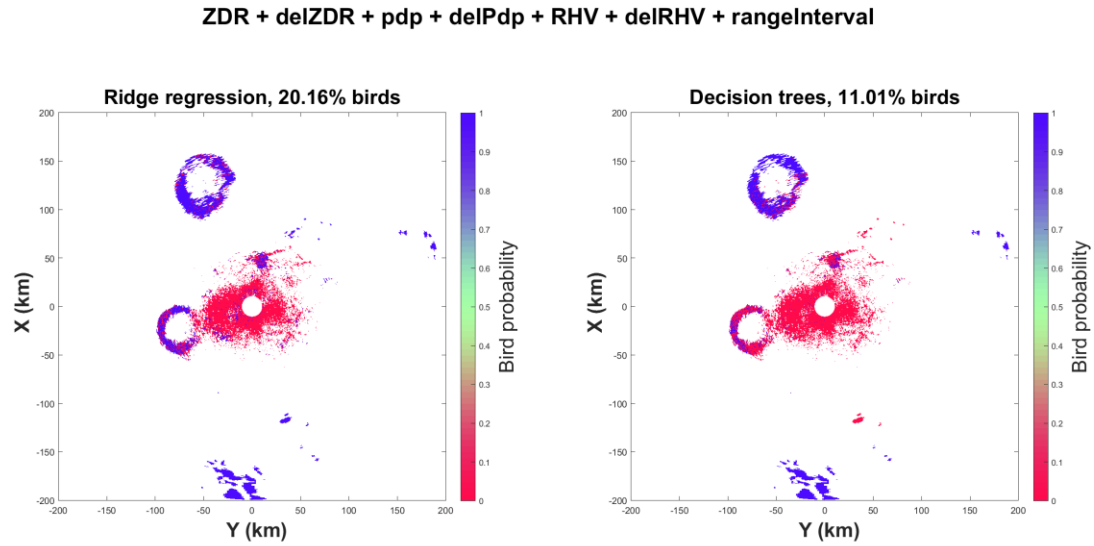

Figure 19: As in Fig. 16, but for different input variables.

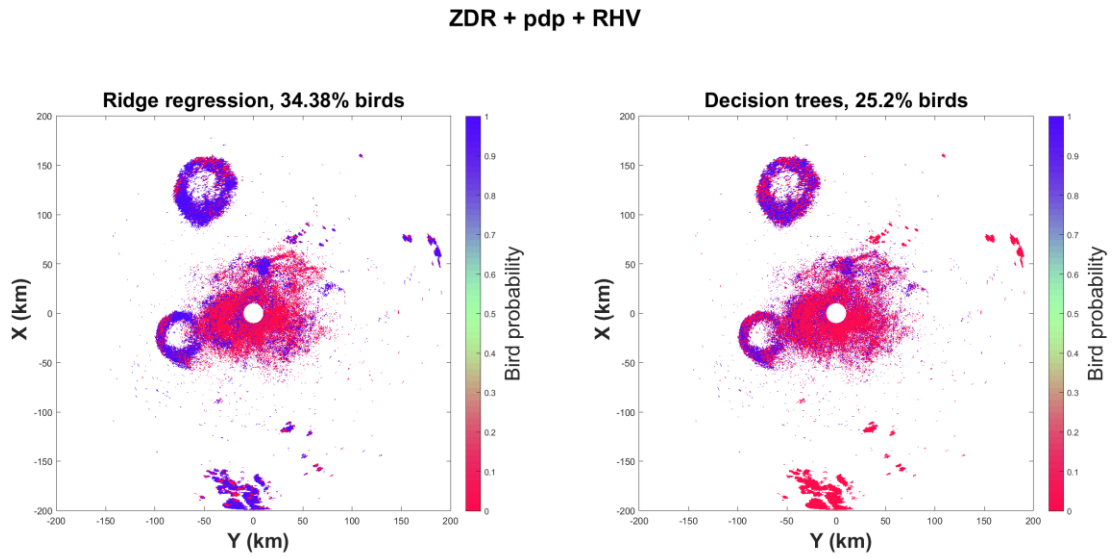

Figure 20: As in Fig. 16, but for different input variables.

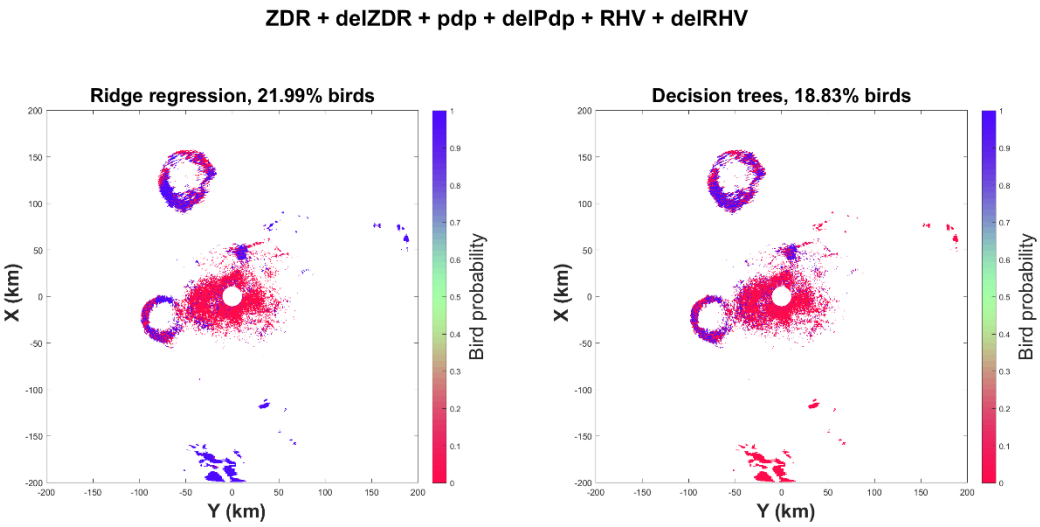

Figure 21: As in Fig. 16, but for different input variables.

5.2. KTLX bird roosts

The second case is for a 0.5° elevation scan collected by KTLX on 08 August 2017. This case was chosen to compare the classification results to the output already obtained from a fuzzy logic classifier (Jatau and Melnikov, 2019). Comparison will be to see what areas the machine learning approach improves upon and also using the fuzzy logic output as validation for our results. We identified four expanding rings which we attributed to birds against a background of insect echoes. The fuzzy logic classifier detected three of these roosts using membership functions of Z, ZDR, Φ_{DP}, and ρ_{HV} from the surveillance scan up to a maximum range of 100 km. A further post processing ZDR threshold of $7.6\ dB$ was applied. All gates with greater ZDR values are classified as insects. All gates with $\rho_{HV} > 0.95$ were also classified as weather echoes (Jatau and Melnikov, 2019). The final classification results are shown in figure 22 below.

While the fuzzy logic approach worked well for separating bird and insect echoes, there are still some drawbacks. The use of reflectivity will aid in detecting bird roosts because there is a dense aggregation of birds. However, it also led to many highly populated insect gates to be misclassified as birds. Hence, the need for human input to correct the results in form of the additional thresholds. Also notice that the fourth roost is not detected because it is outside the 100 km range limit considered.

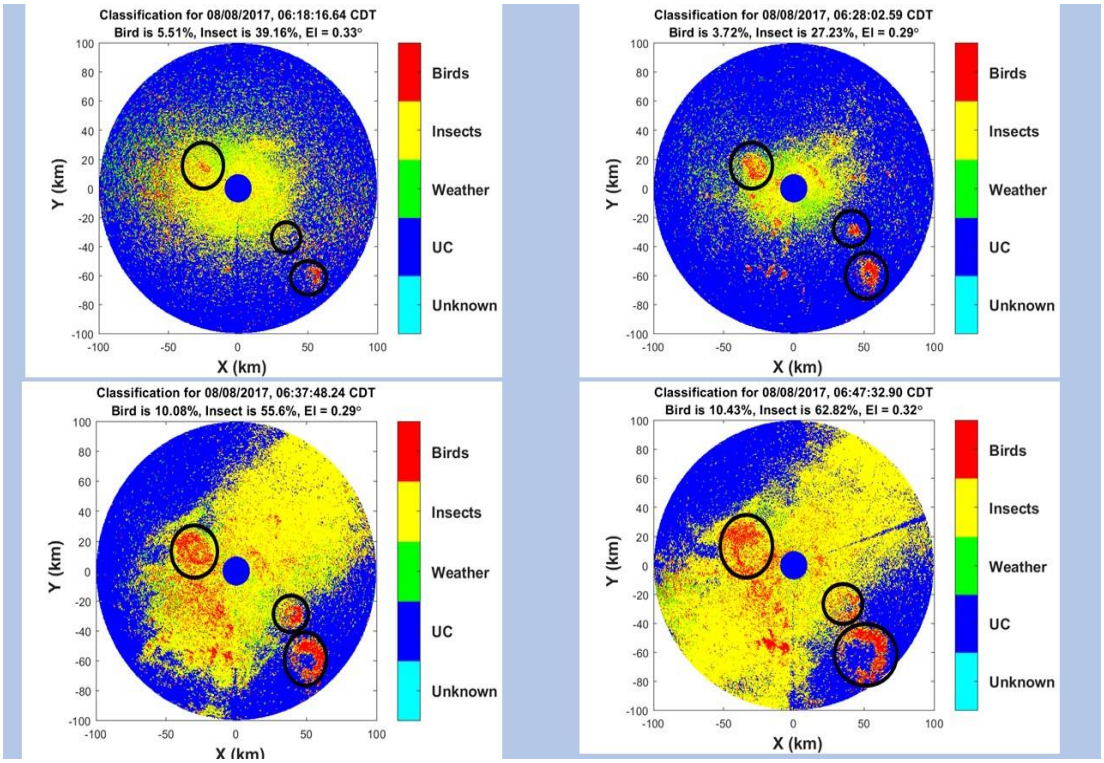

Figure 22: Fuzzy logic classification output for KTLX bird roosts for 08 August 2017. Birds are in red, insects are in yellow. The last case (lower right) was examined using machine learning.

The machine learning classifiers were trained using only dual pol variables which are more robust to the concentration of scatterers within a range gate. They were also trained to detect echoes up to ranges of about 200 km from the radar. The reflectivity image of the 11:47 UTC scan is shown in fig. 23. Fig. 24 shows

the machine learning classification output using only dual pol variables and range interval. It was difficult to obtain sector because of the heterogenous combination of scatterers. The ridge regression model (left) detects birds as the major cause of all the roosts without using any additional post processing step. It also detects the fourth roost which is located about 120 km north-east of the radar. We believe these qualities make it better than the fuzzy logic classifier. Regardless, the similar output for both classifiers despite being based on different methods further affirms our belief in the composition of clear air echoes. We also believe that ridge regression is the best performing machine learning classifier.

The decision tree (fig 24, right) picks up part of the north-east roost and misclassifies most of the south-eastern part of the roosts, which are closer to the radar. This again is the effect of the binary splitting on range so that low ranges tend to be classified as insects. As a result, the boundary between birds and insects at the north eastern roost draws out an unrealistic chord. Figures 25 – 27 shows the results for other models. Generally, ridge regression produces more accurate output than decision tree. Models with texture also do not seem to perform as well. For example, notice that figures 25 and 27 does not clearly pick up the bird roosts.

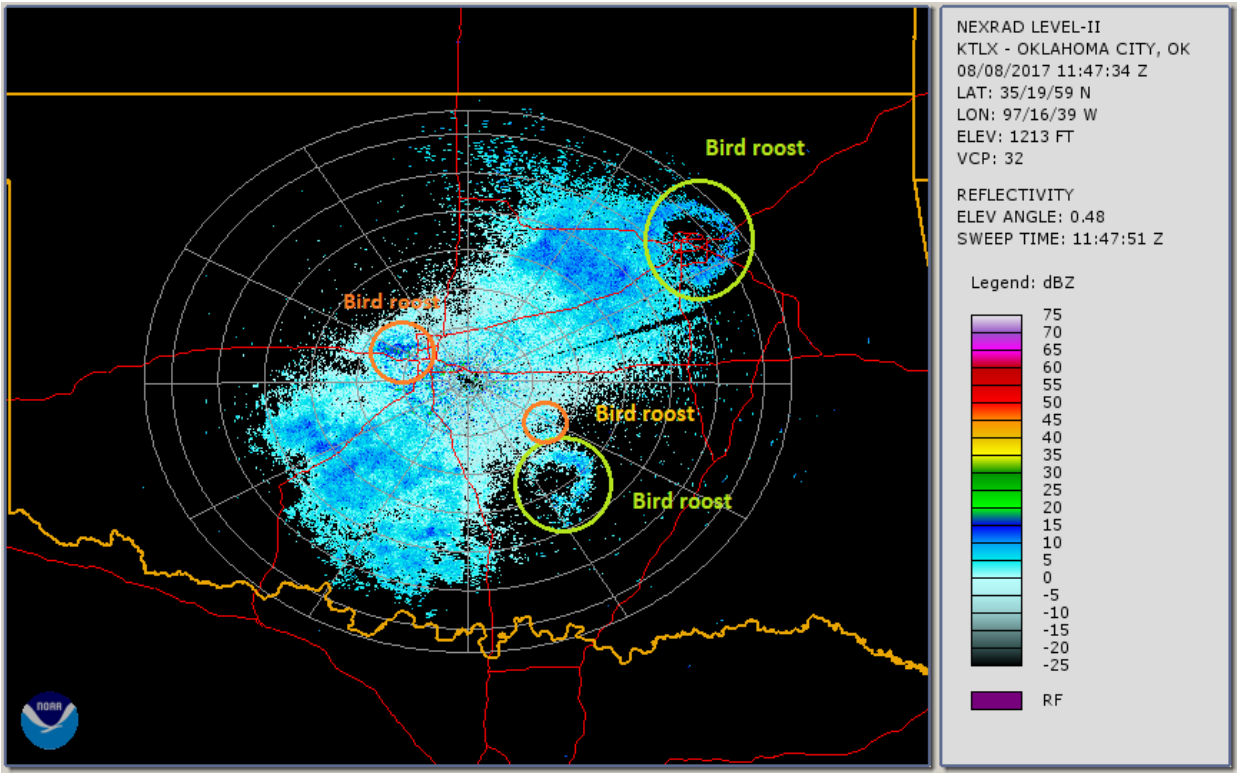

Figure 23: Reflectivity of bird roosts collected by KTLX by 11:47 UTC at 0.5° *on 08 August, 2017.*

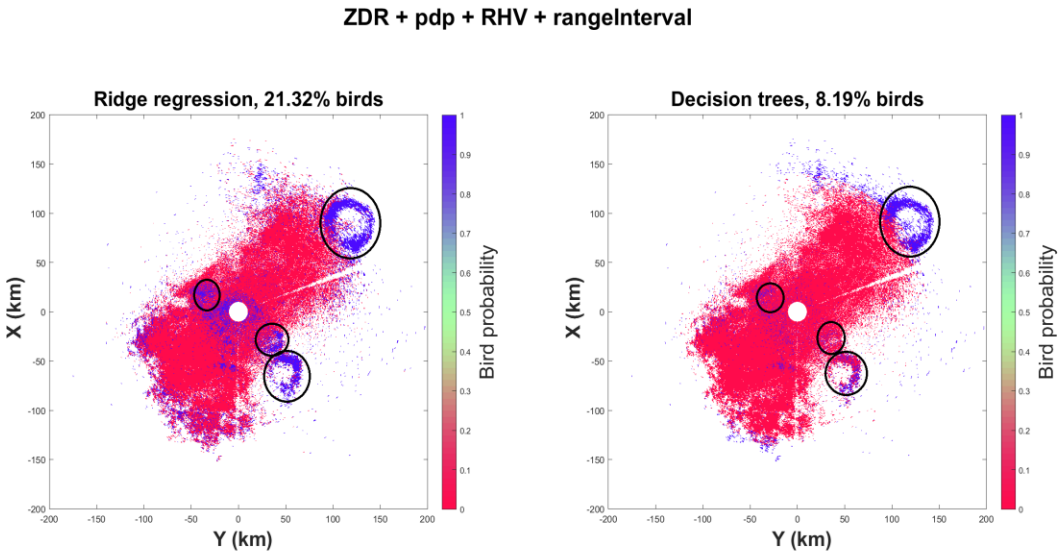

Figure 24: Ridge regression (left) and decision tree (right) classification results using dual pol variables and range interval. The location of the roosts are enclosed within the black circles.

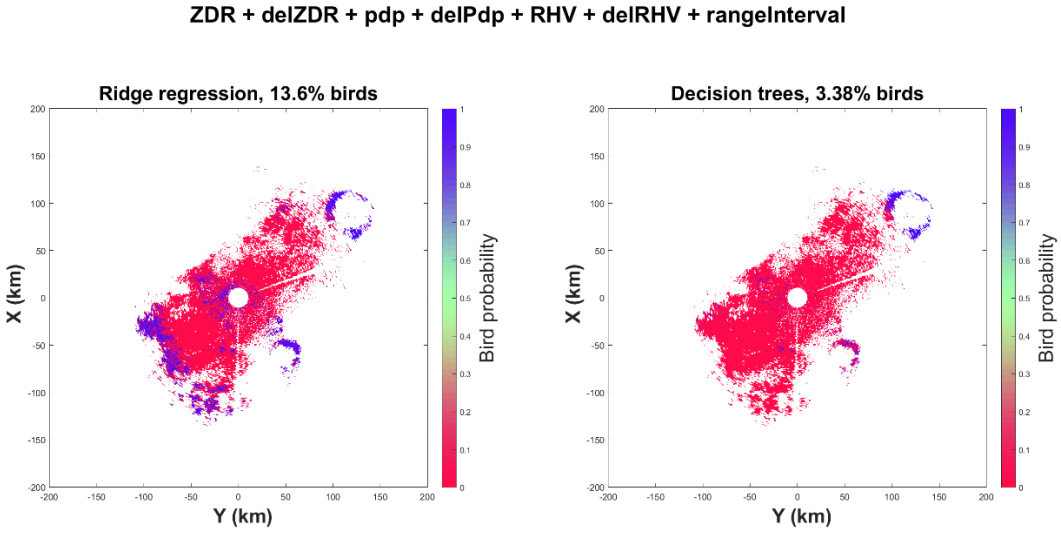

Figure 25: Ridge regression (left) and decision tree (right) classification results using dual pol variables, their textures and range interval

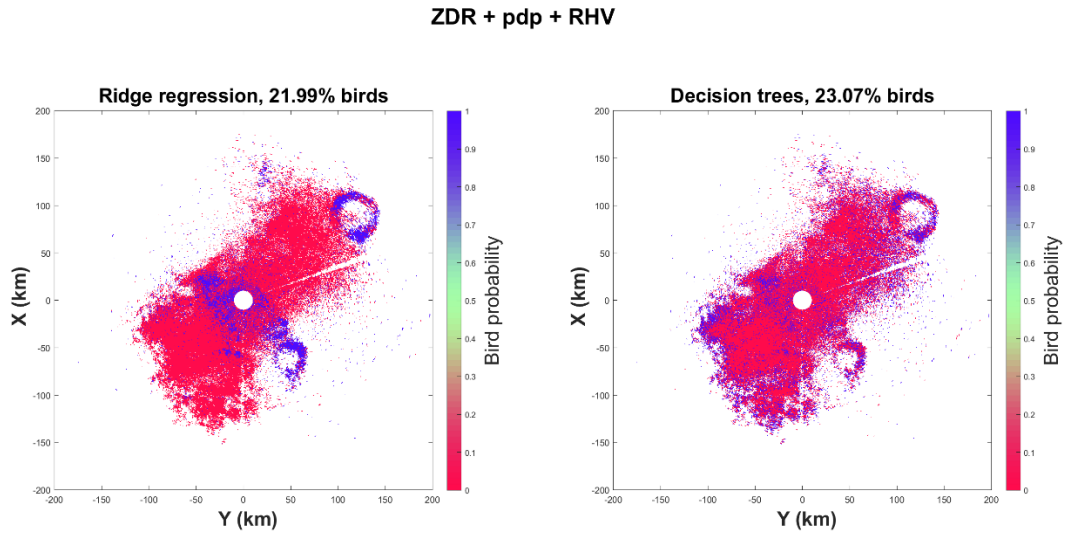

Figure 26: Ridge regression (left) and decision tree (right) classification results using only dual pol variables

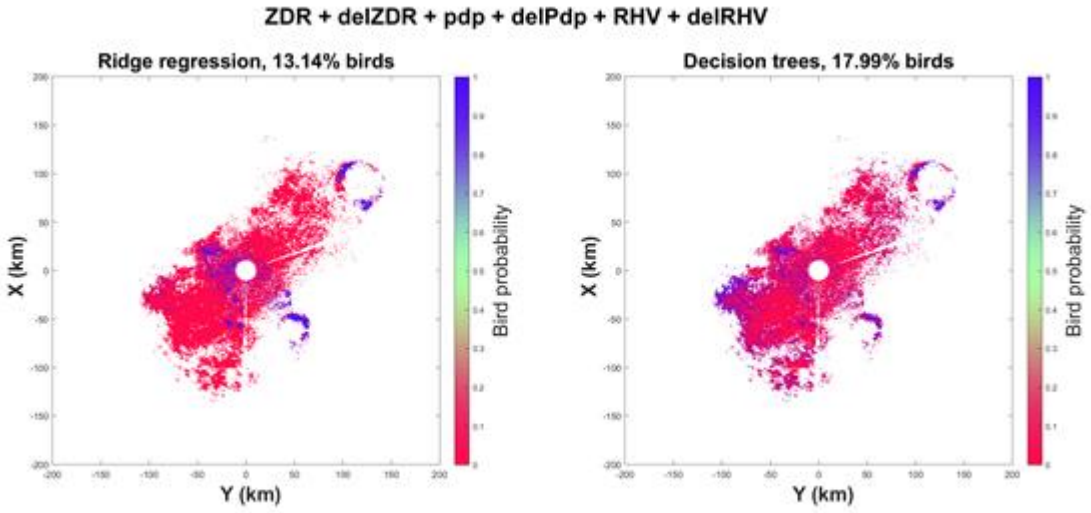

Figure 27: Ridge regression (left) and decision tree (right) classification results using only dual pol variables and their textures

5.3. Bird migration case

The third case is for bird migration collected from the 0.5° elevation scan by KTLX on 03 March 2018. Echoes are assumed to be birds because temperature is too cold for insect activity. Classification using the fuzzy logic classifier (Jatau and Melnikov, 2019) detected birds as the main source of migration for that

night. These results are shown in figure 28. Few insect echoes were also detected close to the radar location.

The Φ_{DP} field for the 04:41 UTC scan is shown in figure 29. This case will be used to analyze the machine learning classifiers. Classification output for dual pol variables and range interval using machine learning are shown in fig. 30. Ridge regression (left) detects 85.26% of gates to be bird dominated with few insects also found close to the radar. This is consistent with the observation of bird migration. Decision trees on the other hand detects 62% of gates to be insects due to its range thresholds. Introduction of texture (fig 31) slightly reduces the proportion of birds detected for both algorithms probably due to most gates with 8 neighbors being located close to the radar. Generally, ridge regression performs better than decision trees for this case.

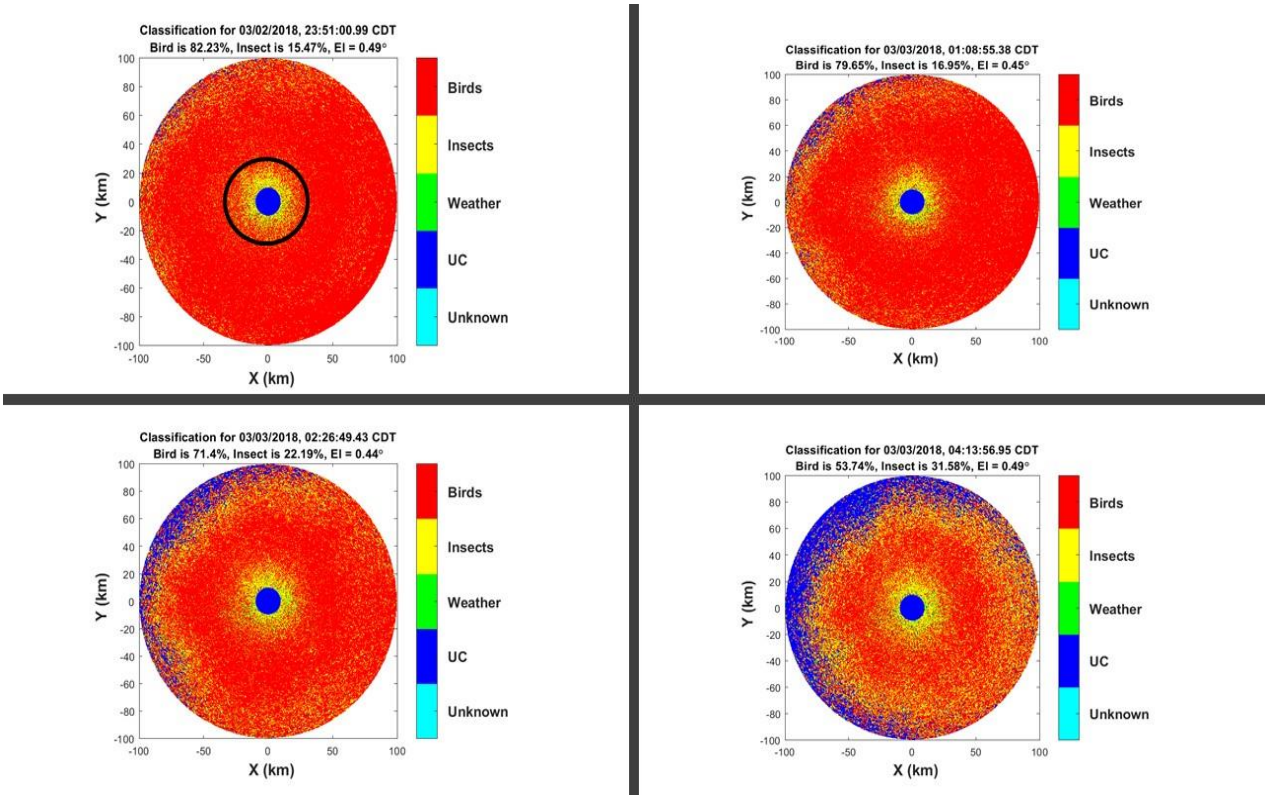

Figure 28: Fuzzy logic classification result for scans between 04:51 UTC and 09:13 UTC. Birds are in red, insects are in yellow. Notice that many insects are detected close to the radar (shown in the black circle).

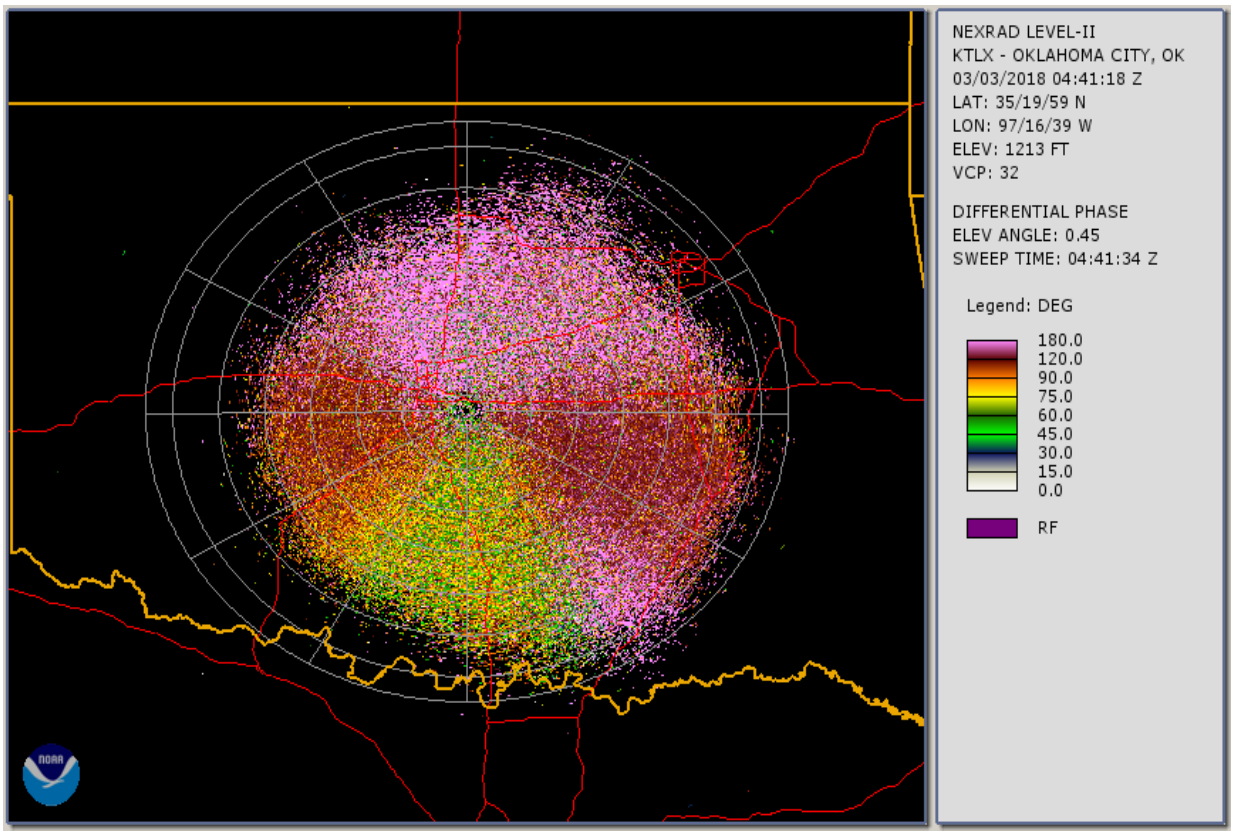

Figure 29: A 0.5° scan for differential phase for measured by KTLX at 04:41 UTC on 03 March, 2018. Echoes were assumed to be birds because temperature is too cold for insect activity.

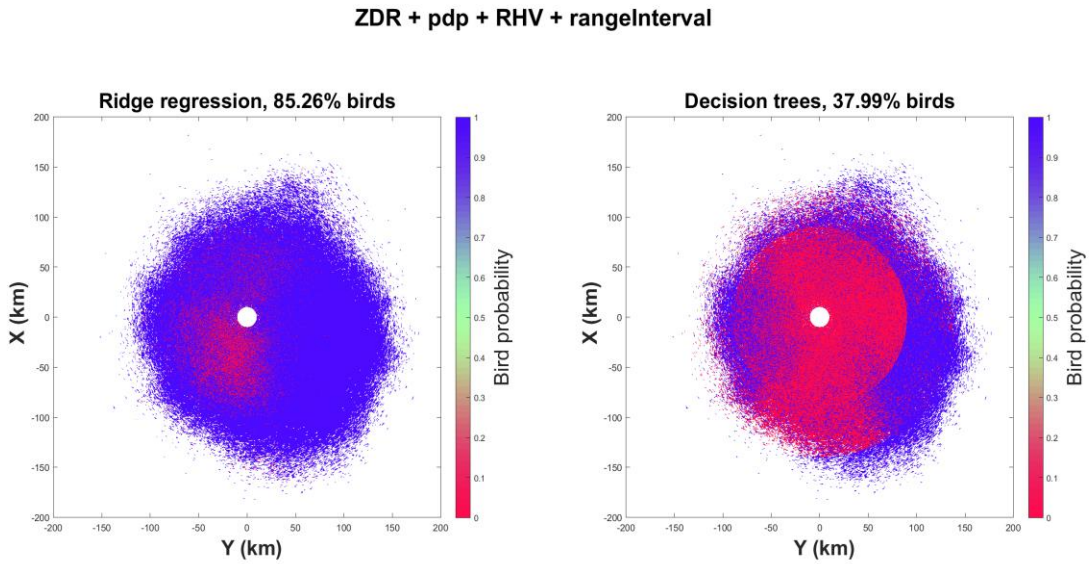

Figure 30: Ridge regression (left) and decision tree (right) classification results using dual pol variables and range interval

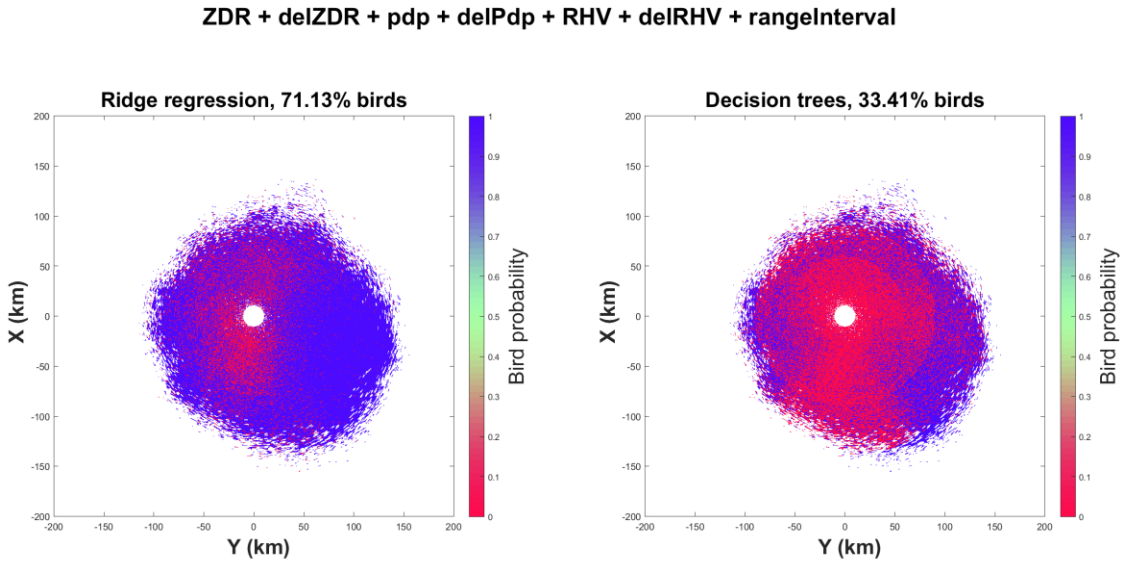

Figure 31: Ridge regression (left) and decision tree (right) classification results using only dual pol variables.

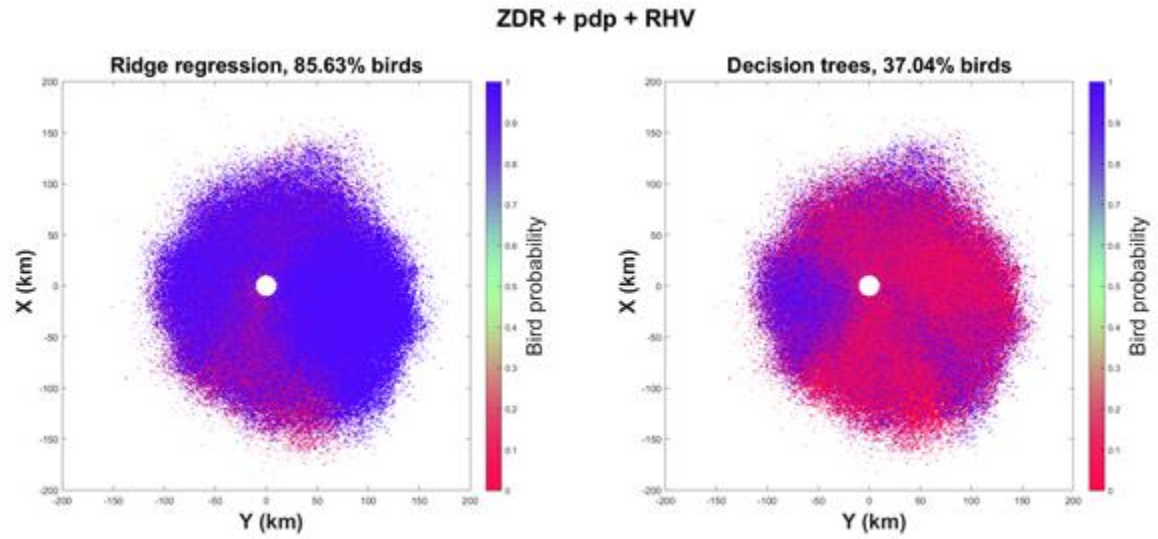

Figure 32: Ridge regression (left) and decision tree (right) classification results using dual pol variables and their textures.

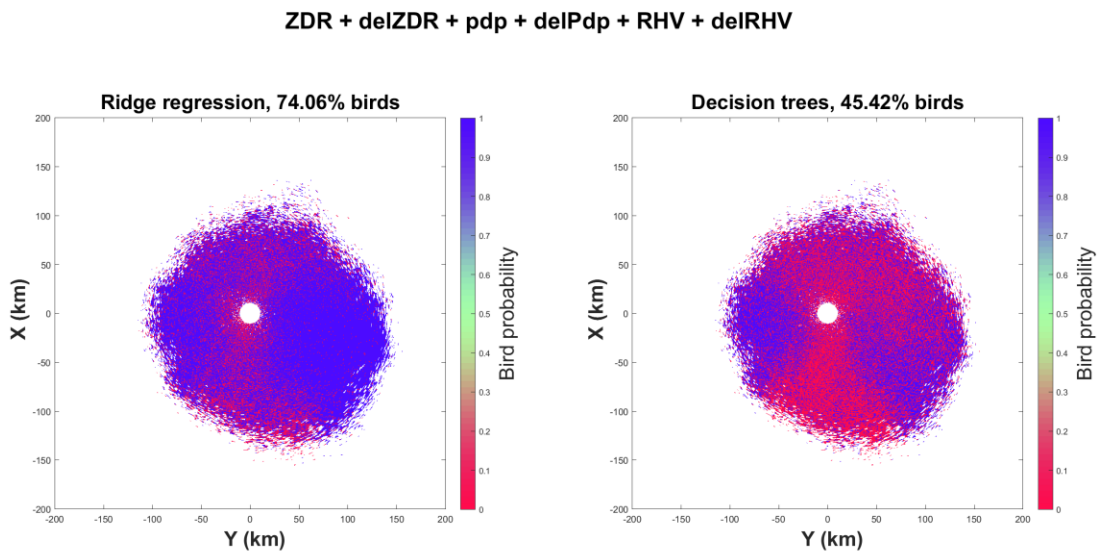

Figure 33: Ridge regression (left) and decision tree (right) classification results using dual pol variables, their textures and range interval

5.4. Insect test case

This case is for insect echoes collected by KTLX at 17:08 UTC on 11 July 2019 at 0.5° elevation. Here migration was toward a defined direction, so sector was obtained. Figure 34 and 35 show classification output for ridge regression and decision trees respectively. Models with range interval detect many bird echoes at the fringe of the migration blob. For ridge regression, the addition of texture worsens the output so that the boundary between birds and insects trace out an artificial circle. This artifact is even worse for similar predictors in the decision tree models (fig. 35) where there is a sharper transition between bird and insect echoes for models with range interval. Ridge regression without texture seem to perform best for these range interval models. For the remaining models however, ridge regression performs better for inputs without textures while decision trees perform better when input textures are added.

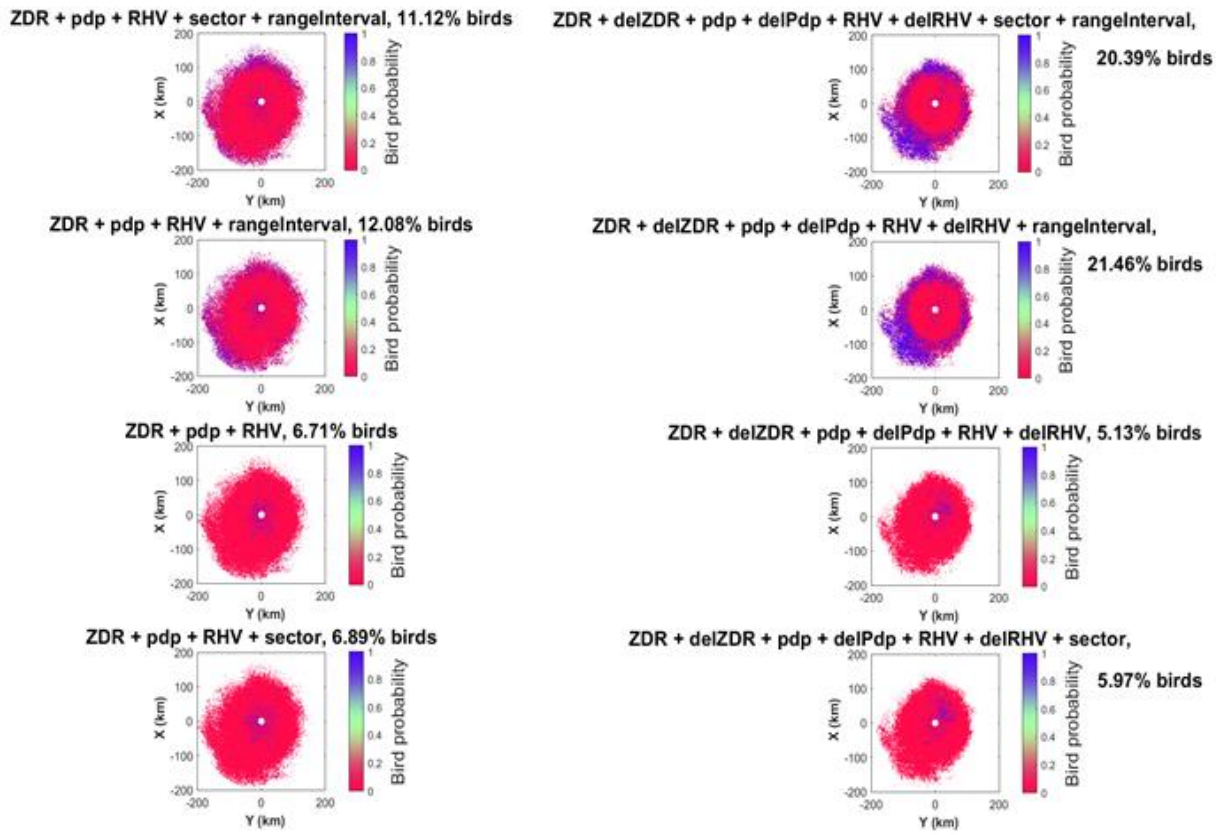

Figure 34: Results of ridge regression on insect test case

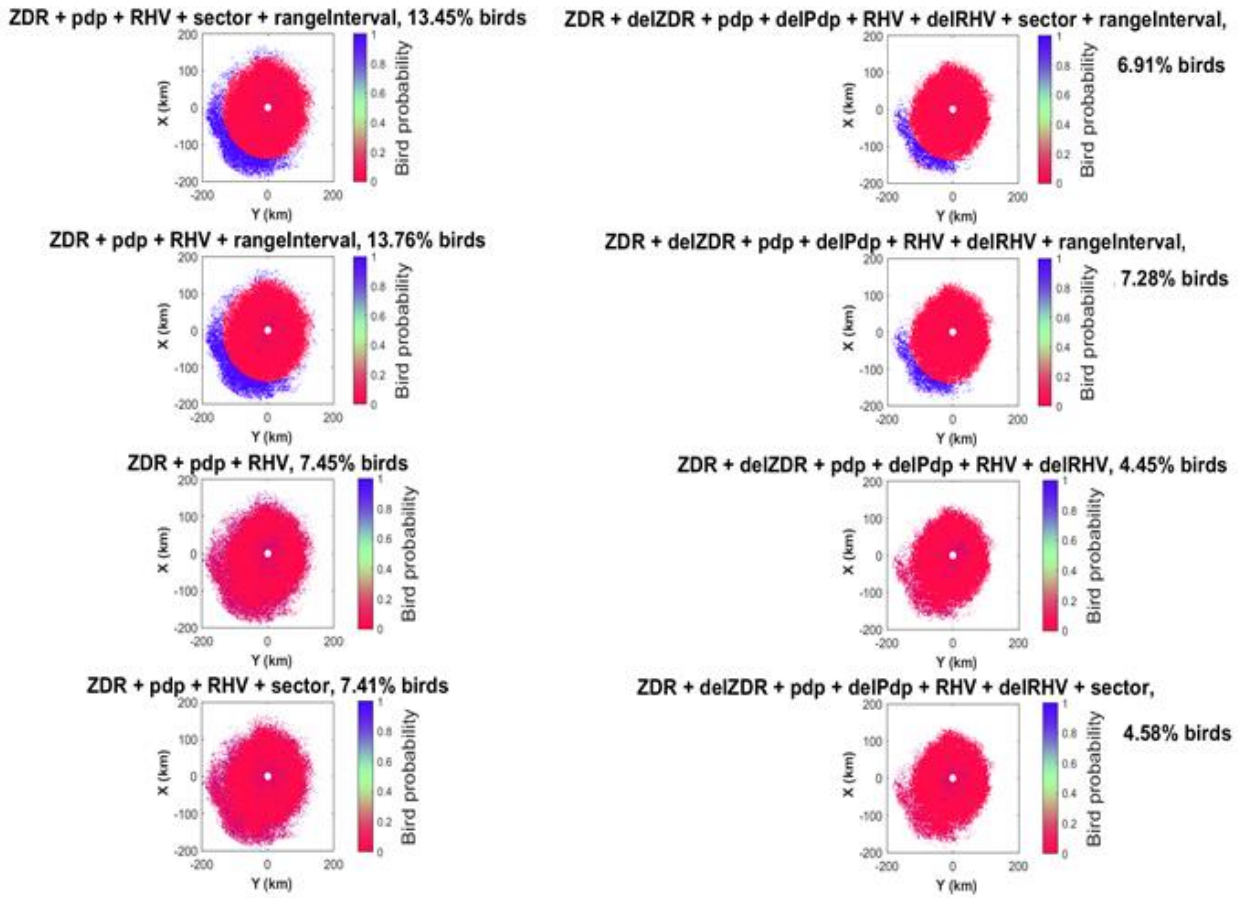

Figure 35: Result of decision trees on insect test case

5.5. Bird test case

The final case is bird echoes collected by KTLX at 04:13 UTC on 2 May 2015 at 0.5° elevation. Sector was also obtained for this case. Fig 36 shows the classification result for the ridge regression model. It outperforms the decision tree model (shown in fig 37) classifying 88.76 – 93.96% of gates as birds compared to 74.83 – 83.69% respectively. Addition of textures in both cases increase the proportion of birds detected for all models except the ridge regression model using dual pol variables and texture. Use of sector in the ridge models also increase the proportion of birds detected.

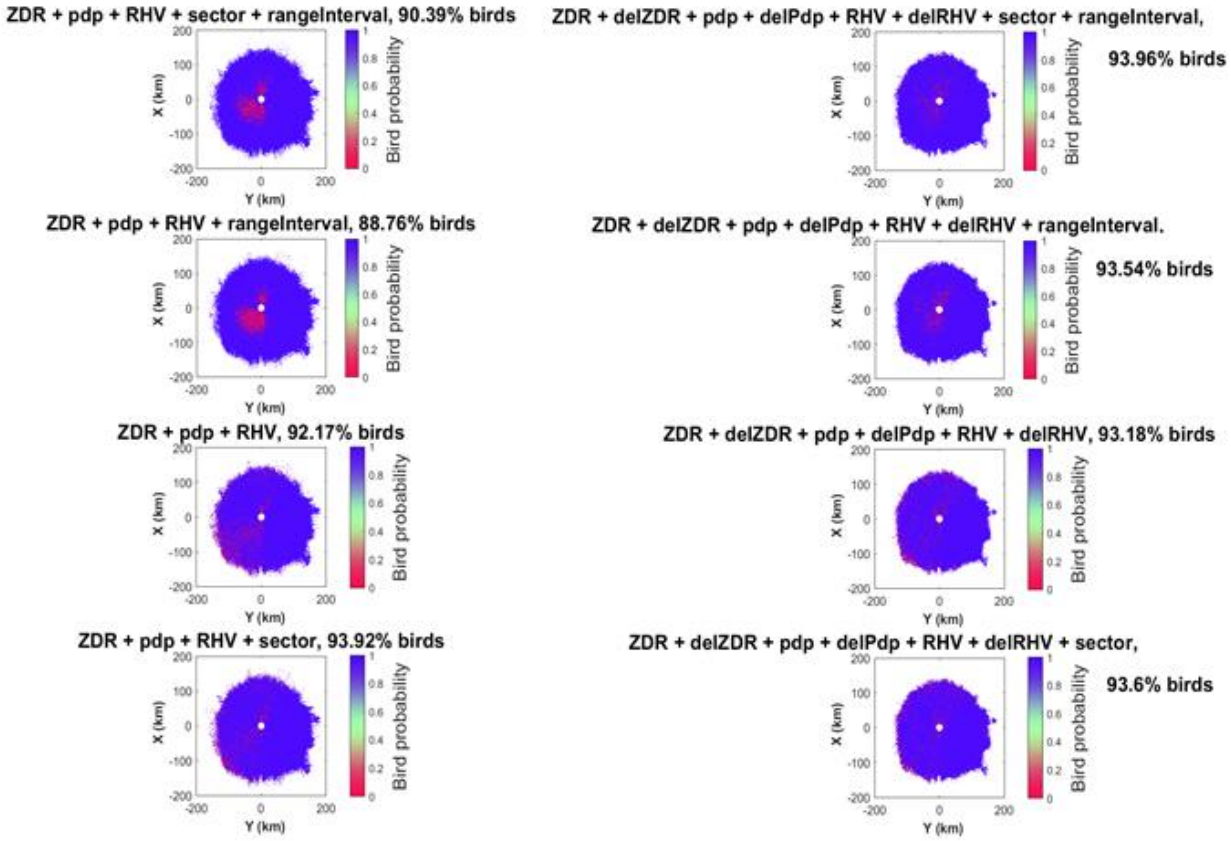

Figure 36: Result of ridge regression on bird test case

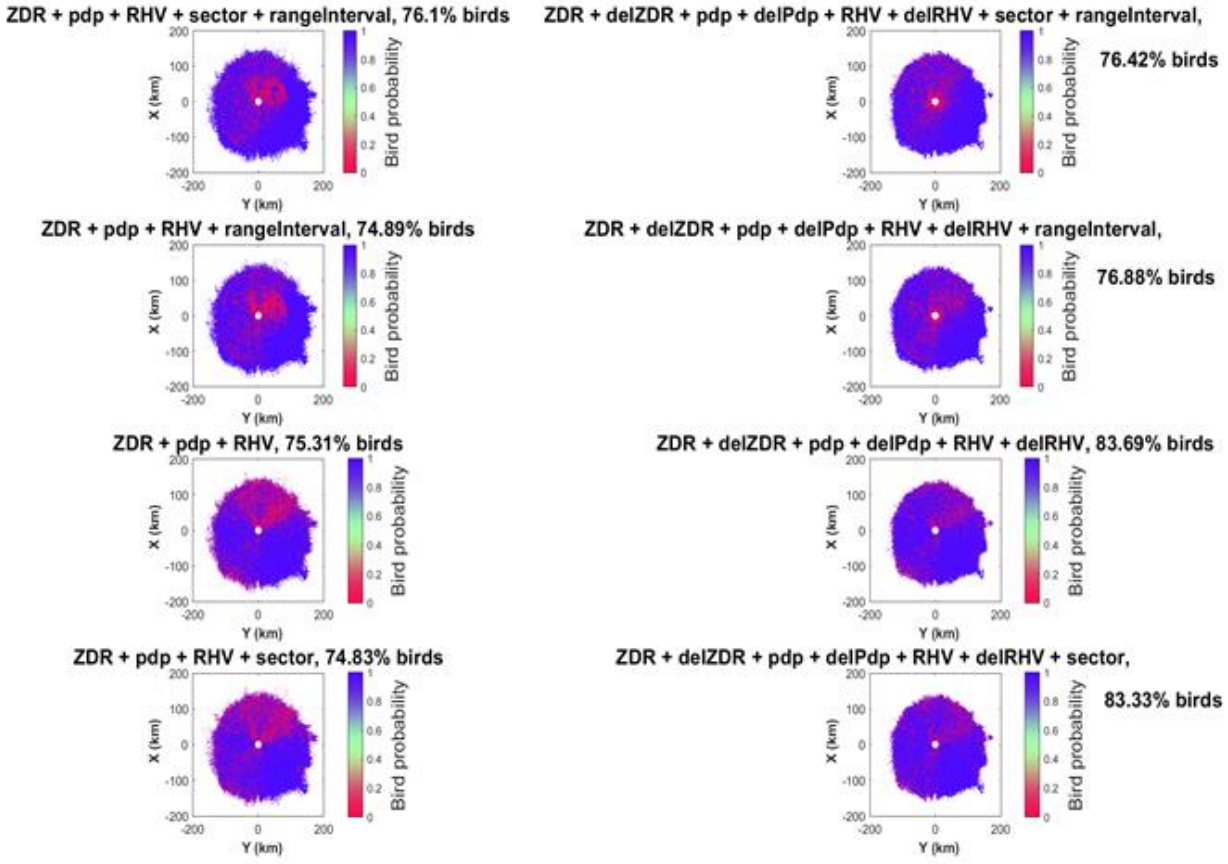

Figure 37: Result of decision trees on bird test case

6. Conclusions

A new method for processing echoes from biological targets has been proposed. It works by leveraging highly directional migration of atmospheric biota to recover the aspect of targets. Aspect averaging on data from 30 ppi's reveal important features of bird and insect radar echoes. Ridge regression and decision trees supervised machine learning classifiers were trained and tested using different combination of dual pol variables, sector and range interval. This variety ensures that classification can be done even when some variables cannot be obtained.

Previous work on bird detection for NEXRAD was based on fuzzy logic (Jatau and Melnikov, 2019). This algorithm used membership functions of Z, ZDR, Φ_{DP} and ρ_{HV} from the surveillance scan and post processing thresholds on ZDR and Φ_{DP} . The fuzzy logic classifier detected the bird roosts obtained in a

0.5° elevation scan collected by KTLX on 08 August 2017 at 11:47 UTC. The use of reflectivity in particular helps detect birds in cases of dense aggregation but is also easily misled by dense population of insects. As a result, it depends on the thresholds used to correct misclassification. The ridge regression classifier is more robust being able to detect these roosts without depending on their concentration (reflectivity) or any additional post processing step.

Another case analyzed was for bird migration collected from the 0.5° elevation scan by KTLX at 04:41 UTC on 03 March 2018. The fuzzy logic classifier detected birds as the main cause of migration on this night with a few insects close to the radar. The ridge regression classifier using dual pol variables and range interval also detects mostly birds (85.3% of range gates) with insects contained at a low height.

Further analysis was carried out to verify if the classifiers can be used for other WSR-88D radars. One case considered was 0.5°elevation scan collected by KHTX on 11 August 2015 at 11:15 UTC. Analysis by Stepanian et al 2016 had verified the composition of these scan. They detected two bird roosts, insects close to the radar and some weather echoes. The ridge regression classifier based on dual pol variables and range interval correctly detects the bird and insect classes. This result shows the potential for applying this algorithm to other WSR-88D radars. Other cases for bird and insect migration were also identified as being dominated by the expected scatterers.

Comparisons was also done between the ridge regression and decision tree methods using classifier metrics. Results showed that the ridge regression algorithm has better performance. This was further highlighted its ability to detect confirmed bird roosts though roosts were not part of the training set. We conclude that the best classifier for separating bird and insect echoes is ridge regression using dual pol variables, range interval and sector for highly directional migration. In the absence of sector, the ridge regression based on dual pol variables and range interval performs best. The latter version will, probably, be used most often. They also have a simple mathematical form that can easily be translated into any programming language. To the best of our knowledge, this is the first machine algorithm that separates bird and insect radar echoes using information from a single range gate without any post processing.

There are many aspects that can be further improved upon. First, collecting more validated data for birds and insects can allow for training at a finer resolution than 10 km in range and 20° in azimuth. There also are more advanced machine learning algorithms that have deeper implementations than the two considered. For instance, the random forest grows a large amount of uncorrelated decision trees and assigns its classification output as the majority vote of this collection. Another possible approach is the neural networks, which use a deep network built on different weighted averages of input variables. Both latter methods should in principle improve classification results. It should be noted however that they are also black box models. More classes of radar echoes like weather, bats and Bragg scatter could also be included in the algorithm for more robust classification.

Acknowledgements

Thanks to Dr Jeffrey Kelly, Dr Kyle Horton and Dr Phillip Stepanian for their valuable contributions to this research project. This project has been funded by the NEXRAD Radar Operations Center.

References

Bovic, A: The Essential Guide to Image Processing. *Burlington, MA: Academic Press (Elsevier), 2009.*

Boulesteix, AL and Fuchs,M (2019). ipflasso: Integrative Lasso with Penalty Factors. *R package version* 0.2. https://CRAN.R-project.org/package=ipflasso

Fawcett, T. 2006. An introduction to roc analysis. *Pattern Recogn. Lett.* 27(8), 861–874.

Federal Aviation Administration. 2016: *Wildlife strikes to Civil Aircraft in the United States 1990 -2015, Report of the Associate Administration or Airports.* National Wildlife Strike Database Serial Report Number 22.

Friedman. J, Hastie. T and Tibshirani. R (2010). Regularization Paths for Generalized Linear Models via Coordinate Descent. *Journal of Statistical Software*, 33(1), 1-22. URL http://www.jstatsoft.org/v33/i01/.

Jatau, P and Melnikov, V., 2019: Classifying bird and insect radar echoes at S-band. 35th Conference on Environmental Information Processing Technologies, Phoenix, Arizona.

Max Kuhn. Contributions from Jed Wing, Steve Weston, Andre Williams, Chris Keefer, Allan Engelhardt, Tony Cooper, Zachary Mayer, Brenton Kenkel, the R Core Team, Michael Benesty, Reynald Lescarbeau, Andrew Ziem, Luca Scrucca, Yuan Tang, Can Candan and Tyler Hunt. (2019). caret: Classification and Regression Training. R package version 6.0-84. https://CRAN.R-project.org/package=caret

Seidenman, P., and Spanovich, D. 2016: *How Bird Strikes Impact Engines*. http://aviationweek.com/author/paul-seidenman-amp-david-j-spanovich.

Sing T, Sander O, Beerenwinkel N, Lengauer T (2005). ROCR: visualizing classifier performance in R. *Bioinformatics*, *21*(20), 7881. <URL: http://rocr.bioinf.mpi-sb.mpg.de>.

Stepanian, P., Horton, K., Melnikov, V., Zrnic, D., and Gauthreaux Jr, S. 2016: Dual polarization radar products for biological applications. *Ecosphere*. 7(11) Article e01539

Stepanian, P. M., and K. G. Horton. 2015. Extracting migrant flight orientation profiles using polarimetric radar. *IEEE Transactions on Geoscience and Remote Sensing* 53:6518–6528.

Therneau,T and Atkinson,B (2018). rpart: Recursive Partitioning and Regression Trees. *R package version* 4.1-13. https://CRAN.R-project.org/package=rpart

Van Den Broeke, M. S. 2013. Polarimetric radar observations of biological scatterers in Hurricanes Irene (2011) and Sandy (2012). *Journal of Atmospheric and Oceanic Technology* 30:2754–2767.

Appendix

All files used in this project can be found in
C:\Users\Precious\Desktop\Research\Summer 2019

The data set for birds
C:\Users\Precious\Desktop\Research\Summer 2019\Radar Data\Birds\45 cases.

Data set for insects
C:\Users\Precious\Desktop\Research\Summer 2019\Radar Data\Insects\45 cases

Matlab scripts for processing features
C:\Users\Precious\Desktop\Research\Summer 2019\Matlab scripts

Averaged training data, test data, trained classifiers, training scripts, testing scripts in both R and matlab
C:\Users\Precious\Desktop\Research\Summer 2019\Models

Classification results
C:\Users\Precious\Desktop\Research\Summer 2019\Models\ViewClassi